

Squalene accumulation in cholesterol auxotrophic lymphomas prevents oxidative cell death

Javier Garcia-Bermudez¹, Lou Baudrier¹, Erol Can Bayraktar¹, Yihui Shen^{2,3}, Konnor La¹, Rohiverth Guarecuco¹, Burcu Yucel¹, Danilo Fiore^{4,5}, Bernardo Tavora¹, Elizaveta Freinkman⁶, Sze Ham Chan⁶, Caroline Lewis⁶, Wei Min^{2,3}, Giorgio Inghirami^{4,5}, David M. Sabatini^{6,7,8,9,10} & Kivanç Birsoy^{1*}

Cholesterol is essential for cells to grow and proliferate. Normal mammalian cells meet their need for cholesterol through its uptake or de novo synthesis¹, but the extent to which cancer cells rely on each of these pathways remains poorly understood. Here, using a competitive proliferation assay on a pooled collection of DNA-barcoded cell lines, we identify a subset of cancer cells that is auxotrophic for cholesterol and thus highly dependent on its uptake. Through metabolic gene expression analysis, we pinpoint the loss of squalene monooxygenase expression as a cause of cholesterol auxotrophy, particularly in ALK⁺ anaplastic large cell lymphoma (ALCL) cell lines and primary tumours. Squalene monooxygenase catalyses the oxidation of squalene to 2,3-oxidosqualene in the cholesterol synthesis pathway and its loss results in accumulation of the upstream metabolite squalene, which is normally undetectable. In ALK⁺ ALCLs, squalene alters the cellular lipid profile and protects cancer cells from ferroptotic cell death, providing a growth advantage under conditions of oxidative stress and in tumour xenografts. Finally, a CRISPR-based genetic screen identified cholesterol uptake by the low-density lipoprotein receptor as essential for the growth of ALCL cells in culture and as patient-derived xenografts. This work reveals that the cholesterol auxotrophy of ALCLs is a targetable liability and, more broadly, that systematic approaches can be used to identify nutrient dependencies unique to individual cancer types.

Cancer cells can be auxotrophic for specific nutrients owing to mutations or decreased expression of metabolic genes^{2,3}. The resulting nutrient dependencies provide potential anti-cancer therapies, with the treatment of leukaemia with L-asparaginase as the clearest example³. Beyond conferring a nutrient dependency, loss of the activity of a metabolic enzyme can also have marked effects on the levels of intermediate metabolites, which may in turn affect non-metabolic cellular processes^{4–6}. Therefore, the identification of cancer nutrient auxotrophies can both inform the development of future therapies and elucidate secondary roles for metabolites.

Cholesterol is a cell-non-essential nutrient because, in addition to being taken up from the environment, it can be synthesized de novo from acetyl-coenzyme A (acetyl-CoA) (Fig. 1a). Although cholesterol auxotrophy is an exceedingly rare phenotypic trait in normal diploid cells^{7,8}, some cancer cell lines are known to depend on exogenous cholesterol for their growth. For example, the histiocytic lymphoma cell line U-937 is cholesterol auxotrophic owing to a defect in 3-ketosteroid reductase (*HSD17B7*)⁷. When incubated in a lipoprotein-depleted serum, U-937 cells die after four days unless supplemented with cholesterol (Fig. 1b, Extended Data Fig. 1a). To determine whether similar cholesterol dependencies are observed in additional cancer cell lines, we undertook a competitive proliferation assay with a pooled collection of 28 cancer cell lines, each marked with a lentiviral-transduced

DNA barcode (Fig. 1c). As lipoproteins are the major carriers of cholesterol in human serum⁹, the pooled population of cell lines was cultured in lipoprotein-replete or lipoprotein-depleted medium for three weeks. Of note, the absence of lipoproteins did not affect the proliferation of most cell lines, suggesting that they can obtain sufficient cholesterol through de novo synthesis (Fig. 1d, Extended Data Fig. 1b, c, Supplementary Table 1). However, lipoprotein depletion did strongly reduce the proliferation of a subset of cancer cell lines, not only U-937, but also U266B1, Raji, Jiyoye and SNU-1—cell lines not previously known to be sensitive to lipoprotein depletion (Fig. 1d, e). In individual growth assays, these cells can proliferate in lipoprotein-depleted conditions when supplemented with free cholesterol, arguing against an essential role for other components of lipoproteins (Extended Data Fig. 1c, d). These data demonstrate that strong extracellular cholesterol dependencies can exist in cancer cells of distinct origins.

Cholesterol biosynthesis occurs through a pathway of over thirty successive steps that converts acetyl-CoA to squalene, which is then cyclized into lanosterol and other downstream sterol compounds¹. Although oncogenic alterations may reprogram cholesterol metabolism in a subset of cancers¹⁰, the presence or absence of such mutations did not correlate with differences in the sensitivity to cholesterol depletion (Extended Data Fig. 1e). We therefore considered that a defect in a cholesterol synthesis gene might render these cells auxotrophic for cholesterol. Analysis of transcriptome-wide gene expression data from the Cancer Cell Line Encyclopedia (CCLE) revealed that one of the cholesterol-dependent cell lines, SNU-1, does not express squalene monooxygenase (*SQLE*) mRNA or SQLE protein (Fig. 2a, Extended Data Fig. 1f, g). Consistent with a block in the *SQLE*-catalysed step of cholesterol biosynthesis, expression of *SQLE* was sufficient to enable the proliferation of SNU-1 cells under cholesterol-depleted conditions (Fig. 2b, Extended Data Fig. 1h). *SQLE* catalyses the conversion of squalene to squalene-2,3-epoxide and is a rate-limiting step in sterol synthesis in mammalian cells¹¹ (Extended Data Fig. 1i). Although squalene, the upstream metabolite in this reaction, is undetectable in most cancer and normal cells, lack of *SQLE* expression results in accumulation of squalene in SNU-1 cells, which further validates the absence of *SQLE* activity (Fig. 2c). Thus, the SNU-1 cell line is a bona fide cholesterol auxotroph because of its lack of *SQLE* activity.

Using gene expression data from the CCLE, we identified nine additional cell lines without detectable *SQLE* mRNA and *SQLE* protein. Of note, six of these cell lines (SU-DHL-1, KIJK, SUP-M2, DEL, SR-786 and Karpas299) belong specifically to the cancer subtype ALK⁺ ALCLs (Fig. 2d, e). Similar to SNU-1, *SQLE*-deficient ALCL cell lines are sensitive to cholesterol depletion (Fig. 2f) and accumulate high amounts of squalene (Fig. 2g). Chemical imaging using stimulated Raman scattering (SRS) microscopy further revealed that, whereas control cells lack squalene, ALCLs accumulate it in lipid droplets (Fig. 2h, Extended

¹Laboratory of Metabolic Regulation and Genetics, The Rockefeller University, New York, NY, USA. ²Department of Chemistry, Columbia University, New York, NY, USA. ³Kavli Institute for Brain Science, Columbia University, New York, NY, USA. ⁴Department of Pathology and Laboratory Medicine, Weill Cornell Medical College, New York, NY, USA. ⁵Department of Molecular Biotechnology and Health Sciences, University of Turin, Turin, Italy. ⁶Whitehead Institute for Biomedical Research, Cambridge, MA, USA. ⁷Howard Hughes Medical Institute and Department of Biology, Massachusetts Institute of Technology, Cambridge, MA, USA. ⁸The David H. Koch Institute for Integrative Cancer Research at MIT, Cambridge, MA, USA. ⁹Department of Biology, Massachusetts Institute of Technology, Cambridge, MA, USA. ¹⁰Broad Institute of Harvard and MIT, Cambridge, MA, USA. *e-mail: kbirsoy@rockefeller.edu

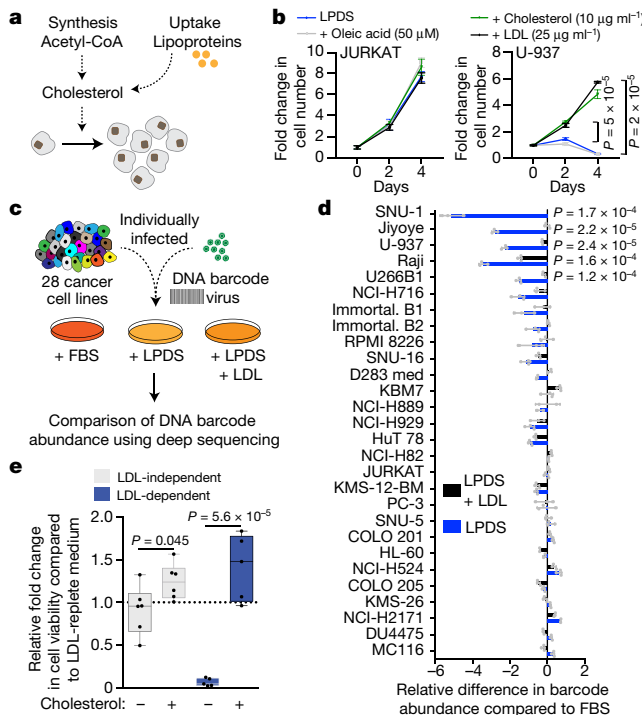


Fig. 1 | Identification of cholesterol auxotrophic cancer cell lines using a barcode-based competition assay. **a**, Cholesterol metabolism in mammalian cells. **b**, Fold change in cell number of Jurkat and U-937 cells cultured with the indicated concentrations of cholesterol, LDL and oleic acid. **c**, Experimental design outline of cell competition assay: 28 cancer cell lines were barcoded with individual DNA barcodes and cultured for 2 weeks in medium supplemented with FBS, LPDS or LPDS + LDL (25 $\mu\text{g ml}^{-1}$). FBS, fetal bovine serum; LPDS, lipoprotein-depleted serum. **d**, Relative difference in barcode abundance of indicated cell lines in the competition assay grown under LPDS-supplemented medium with (black) and without (blue) LDL, relative to FBS. **e**, Relative fold change in cell number of LDL-independent (grey) and LDL-dependent (blue) cell lines in the presence or absence of cholesterol. **b**, **d**, Bars represent mean \pm s.d.; **e**, boxes represent the median, and the first and third quartiles, and the whiskers represent the minimum and maximum of all data points. **b**, $n = 3$ biologically independent samples; **d**, $n = 3$ independent barcodes per cell line; **e**, $n = 5–6$ biologically independent cell lines. Statistical significance was determined by two-tailed unpaired *t*-test.

Data Fig. 2a, b). Loss of SQLE expression is associated with promoter hypermethylation, and treatment with DNA-hypomethylating agents upregulates SQLE mRNA expression (Extended Data Fig. 2c–e). We next investigated whether SQLE downregulation is also a feature of primary tumour samples and patient-derived tumour xenografts (PDXs) of ALK⁺ ALCLs. Analysis of previously published mRNA expression data from ALCLs¹² and quantitative PCR of primary tumour samples revealed that *SQLE* is indeed one of the most significantly differentially expressed genes in primary ALK⁺ ALCL tumours compared to ALK⁻ ALCLs (Fig. 2i, Extended Data Fig. 3a, b, Supplementary Table 2). In agreement with the mRNA data, we observed a marked reduction of SQLE protein levels in primary ALK⁺ ALCL tumours compared to other lymphoma types (Extended Data Fig. 3c–e). Despite highly significant inverse correlation between NPM–ALK translocation and SQLE expression, modulation of ALK signalling did not affect SQLE expression, which suggests that SQLE may be silenced owing to a different mechanism (Extended Data Fig. 3f–h). Altogether, these results demonstrate that ALK⁺ ALCLs lack SQLE expression and thus are cholesterol auxotrophs.

Given the strong cholesterol dependency of ALK⁺ ALCLs, we next explored whether this unexpected metabolic feature could be exploited as a therapeutic vulnerability. Using a focused CRISPR library targeting 200 core metabolic enzymes (Supplementary Table 3), we performed

a negative selection screen to identify genes the loss of which inhibits the fitness of cholesterol auxotrophic ALK⁺ ALCL cells but not of their SQLE-expressing counterparts or a prototrophic cell line (Fig. 3a, Extended Data Fig. 4a). The highest scoring gene in these screens was the low-density lipoprotein (LDL) receptor (*LDLR*) (Fig. 3b, Extended Data Fig. 4b–d, Supplementary Table 4). *LDLR* provides a major source of cholesterol for mammalian cells by serving as the cell-surface receptor for the endocytosis of cholesterol-rich LDL^{1,9}. Consistent with the screen results and the essential role of *LDLR* in the survival of ALCLs, depletion of *LDLR* using a conditional CRISPR–Cas9 system (Fig. 3c, Extended Data Fig. 4e–i) or targeting it with a monoclonal anti-*LDLR* antibody (Extended Data Fig. 4j–l) strongly decreased the proliferation of ALK⁺ ALCL lines but not of control cells. ALK⁺ ALCLs upregulate *LDLR*-mediated cholesterol uptake (Extended Data Fig. 5a) and expression of cholesterol uptake genes (Fig. 3d, Extended Data Fig. 5b–e) to compensate for their deficiency in de novo cholesterol biosynthesis, an adaptation essential for ALK⁺ ALCL cells to proliferate. Consistent with these findings, CRISPR–Cas9-mediated *LDLR* depletion inhibited the growth of mouse tumour xenografts derived from ALK⁺ ALCL cancer cell lines (DEL and Karpas299) but not that of a control cell line (KMS-26) (Fig. 3e). To translate our findings to a more relevant *in vivo* model, we asked whether targeting *LDLR* affects the growth of PDXs. For this, we performed an *in vivo* loss-of-function competition assay using a pool of single guide RNAs (sgRNAs) targeting control genomic regions or the *LDLR* gene. The sgRNAs targeting the *LDLR* gene strongly inhibited the growth of tumours derived from the DEL cell line as well as from three different ALK⁺ ALCL PDXs, but not that of isogenic tumours expressing SQLE (Fig. 3f). Collectively, our data identify cholesterol uptake through *LDLR* as a therapeutic target for ALK⁺ ALCLs *in vivo*.

We reasoned that a decrease in cholesterol synthesis was unlikely to confer an advantage to cancer cells and so investigated whether loss of SQLE activity might have other beneficial effects on ALCL metabolism and growth. As the accumulation of certain metabolites in cancer cells can promote tumorigenesis by altering cellular processes distinct from the original metabolic pathways in question^{4,6,13}, we focused our attention on squalene, a relatively poorly characterized metabolic intermediate that accumulates at very high levels upon SQLE loss (Fig. 2g). Squalene is a main component of human sebum and is proposed to have a role as an emollient and a natural antioxidant for the skin, but the role of squalene in cancer biology has been poorly explored^{14,15}. To understand the metabolic consequences of squalene accumulation in ALCLs, we genetically targeted squalene synthase (*FDFT1*), the enzyme immediately upstream of SQLE in cholesterol biosynthesis responsible for the synthesis of squalene. CRISPR–Cas9-mediated knockout of *FDFT1* blocked squalene synthesis, and returned squalene to levels seen in non-ALCL cells (Fig. 4a, b, Extended Data Fig. 6a, b). To test whether squalene accumulation in ALK⁺ lymphomas is beneficial for tumour formation *in vivo*, we generated tumours by injecting *FDFT1*-knockout Karpas299 cells expressing a vector or an sgRNA-resistant *FDFT1* cDNA subcutaneously into immunodeficient mice. Loss of *FDFT1* caused a marked decrease in the size of Karpas299 tumours (Fig. 4c). Similarly, competition experiments using *FDFT1* and control sgRNAs in two ALK⁺ PDX models showed a significant depletion of *FDFT1* sgRNAs (Extended Data Fig. 6c). These data suggest that squalene synthesis may be beneficial for optimal growth of ALK⁺ ALCLs *in vivo*.

We next investigated how squalene may affect cellular metabolism in ALK⁺ ALCLs. As accumulation of lipid peroxides are detrimental to cell viability, most mammalian cells repair lipid damage using the phospholipid peroxidase glutathione peroxidase 4 (GPX4), inhibition of which causes ferroptosis, a recently described form of cell death^{16–18}. Squalene is a lipophilic metabolite that can accumulate in cellular membranes and lipid droplets (Fig. 2h, Extended Data Fig. 2b). We therefore investigated whether squalene may be protective of lipid peroxidation and ferroptotic cell death. Blocking squalene accumulation by genetic loss of *FDFT1* (Fig. 4d, Extended Data Fig. 6d–g) or

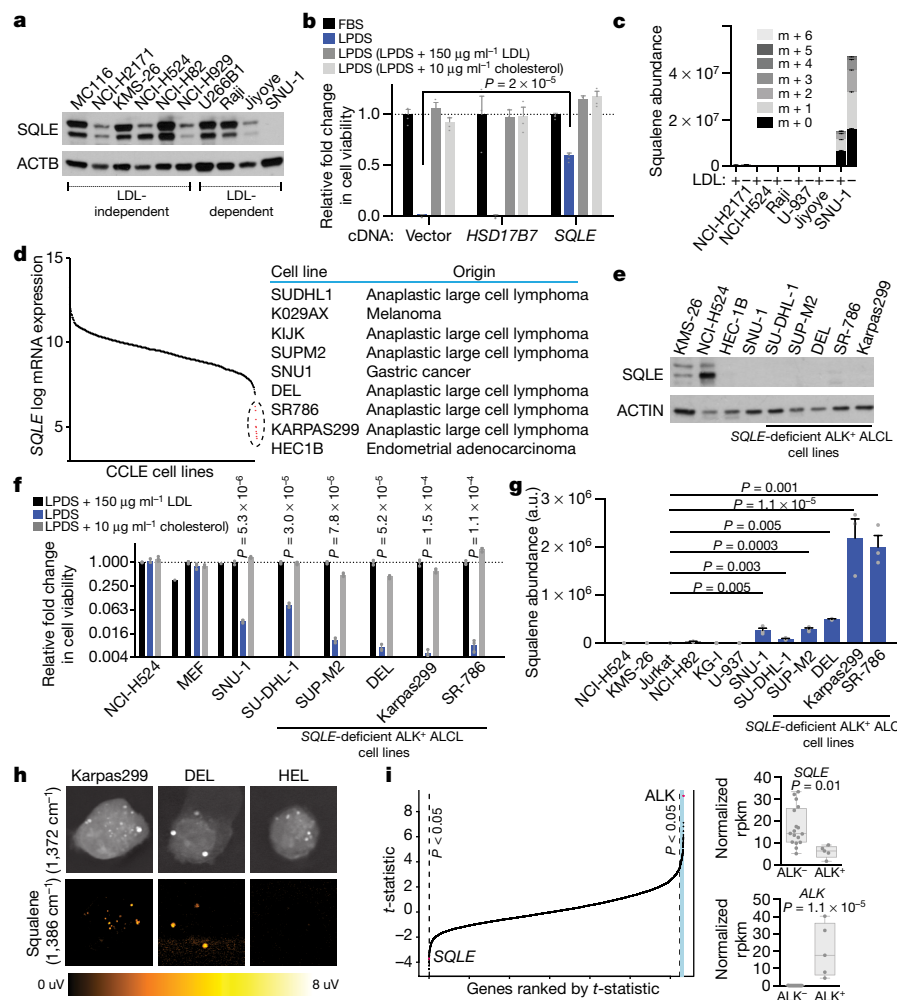


Fig. 2 | ALK⁺ ALCLs are auxotrophic for cholesterol owing to a lack of SQLE expression. **a**, Immunoblotting for SQLE in LDL-dependent and independent cancer cell lines. Actin was used as a loading control. **b**, Relative fold change in cell viability of control and SQLE- or HSD17B7-expressing SNU-1 cancer cells grown for five days under LPDS in the absence or presence of LDL or cholesterol. **c**, Mass isotopomer analysis of squalene in indicated cancer cell lines in the presence or absence of LDL after a 24-h incubation with [$U-^{13}C$]acetate. **d**, Expression levels of *SQLE* mRNA in 1,037 cell lines from CCLE database. Cell lines with undetectable *SQLE* mRNA levels and their tissue origins are indicated. **e**, Immunoblotting for SQLE in ALK⁺ ALCL and control cancer cell lines. Actin was used as the loading control. **f**, Relative fold change in cell viability of indicated cancer cell lines grown for five days with LPDS in the absence and presence of LDL or cholesterol. **g**, Squalene abundance in

control and SQLE-deficient cancer cell lines. **h**, Raman spectra of squalene and cholesterol for the indicated cell lines. SRS images were obtained at squalene channel ($1,386 \text{ cm}^{-1}$) and at lipid channel ($1,372 \text{ cm}^{-1}$) in the same cell. **i**, Genes ranked by differential expression analysis of primary ALK⁺ ALCL primary samples compared to ALK⁻ samples (left). Student's *t*-test statistic of each gene was ranked as a function of its *t*-test rank. ALK⁻ and ALK⁺ normalized expression (rpkm, reads per kilobase of million) of *SQLE* and *ALK* are indicated (right). **b**, **c**, **f**, **g**, Bars represent mean \pm s.d.; **i**, boxes represent the median, and the first and third quartiles, and the whiskers represent the minimum and maximum of all data points. **b**, **c**, **f**, **g**, $n = 3$ biologically independent samples; **i**, $n = 17$ biologically independent ALK⁻ samples, 5 biologically independent ALK⁺ samples. Statistical significance was determined by two-tailed unpaired *t*-test.

small molecule inhibitors (Extended Data Fig. 7) sensitized SQLE-deficient cells to ferroptosis induced by GPX4 inhibitors (ML162 and RSL3). Extracellular squalene supplementation fails to provide this protective phenotype, which suggests that squalene may need to accumulate in the right cellular compartments for its function (Extended Data Fig. 8). Consistent with cell death by ferroptosis, the addition of an antioxidant (ferrostatin-1) or blocking long-chain polyunsaturated fatty acid (PUFA) incorporation into membrane lipids by knocking out acyl-CoA synthetase long-chain family member 4 (ACSL4)¹⁹ eliminated the sensitivity of FDFT1-knockout ALCLs to GPX4 inhibitors (Fig. 4d, Extended Data Fig. 9a–c). Similarly, expression of *SQLE* cDNA in ALCL cells decreased squalene levels, sensitized them to GPX4 inhibitors and blunted *in vivo* tumour growth (Fig. 4b–d, Extended Data Fig. 6a, d, e). Additionally, a decrease in squalene levels upon FDFT1 loss or SQLE overexpression increased lipid reactive oxygen, a hallmark of ferroptosis rescued by antioxidants when cells were treated with ferroptosis

inducers (Extended Data Fig. 9d, e). As membrane PUFAs are highly susceptible to damage by oxidation¹⁹, squalene accumulation may protect these membrane lipids from chemical modification or rewire membrane lipid composition, thereby providing a survival advantage to them under oxidative stress. Reflective of the protective role of squalene, loss of squalene accumulation enhanced the depletion of membrane PUFAs containing arachidonic acid (AA, 20:4), adrenic acid (Ada, 22:4) and docosahexaenoic acid (DHA, 22:6) in FDFT1-null cells on ML162 treatment (Fig. 4e, Extended Data Fig. 10a–c). Although an increase in the levels of GPX4 protein or coenzyme Q^{20,21} by inhibition of the lower sterol synthesis pathway can protect against lipid peroxidation (Extended Data Fig. 10d), we did not observe a change in levels of GPX4 protein or coenzyme Q in ALK⁺ ALCLs on FDFT1 loss (Extended Data Figs. 7, 10e–f). Therefore, our findings reveal that squalene is a lipophilic metabolite that is elevated in ALK⁺ ALCLs and can prevent damage of membrane PUFAs under oxidative stress.

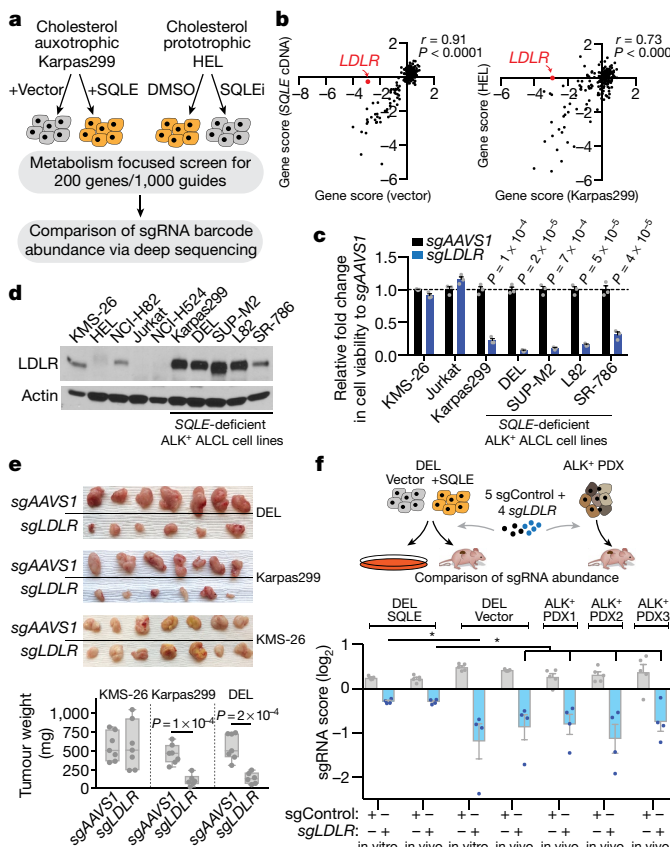


Fig. 3 | In ALK⁺ ALCLs *LDLR* is upregulated and is potential therapeutic target. **a**, Schematic for CRISPR-Cas9-based negative selection screening. SQLEi, SQLE inhibitor. **b**, Comparison of gene essentiality between indicated cancer cell lines. Pearson correlation coefficients are indicated. Red dot denotes *LDLR*. **c**, Relative fold change in cell viability of indicated cancer cell lines infected with sgRNAs targeting *AAVS1* or *LDLR* and grown for five days. **d**, Immunoblot of *LDLR* in the indicated cancer cell lines. Actin was used as the loading control. **e**, Representative images (top) and weights (bottom) of subcutaneous tumour xenografts derived from indicated cancer lines expressing sgRNAs targeting *AAVS1* or *LDLR* after four weeks of growth. **f**, Mini sgRNA competition assay using a pool of control (sgControl) and *LDLR*-targeting (sg*LDLR*) sgRNAs in indicated cancer cell lines and PDXs. Average guide scores of tumours and cell lines were calculated and graphed. *P < 0.05. **c, f**, Bars represent mean \pm s.d.; **e**, the boxes represent the median, and the first and third quartiles, and the whiskers represent the minimum and maximum of all data points; **c**, n = 3 biologically independent samples; **e**, n = 6, 7 biologically independent samples. For **f**, n = 5 independent sgRNAs targeting a control region and 4 sgRNAs targeting the *LDLR* gene. Statistical significance was determined by two-tailed unpaired t-test.

Cancer-associated alterations in metabolic enzymes influence the levels of metabolic intermediates and may thereby affect non-metabolic cellular functions such as signalling and the epigenetic state^{5,13}. For example, succinate and fumarate accumulate in cancers with SDH or FH mutations and may exert their pro-tumorigenic effects by acting as epigenetic modulators^{22,23}. Here we find that ALK⁺ ALCLs lose squalene monooxygenase activity and accumulate squalene, a metabolite with antioxidant-like properties (Fig. 4f). As activation of cellular antioxidant defence is selected for in some tumour types²⁴ or under certain stresses^{21,25,26} and may protect cancer cells from ferroptosis²⁷, SQLE suppression may be an additional mechanism underlying this cancer hallmark. Future work is required to understand the role of squalene accumulation in cancer initiation and progression. In addition, our work identifies cholesterol auxotrophy of ALK⁺ ALCLs as a targetable metabolic liability and adds ALCLs to the small list of cancers that are selectively auxotrophic for a particular nutrient. As a block in LDL uptake inhibits the growth of

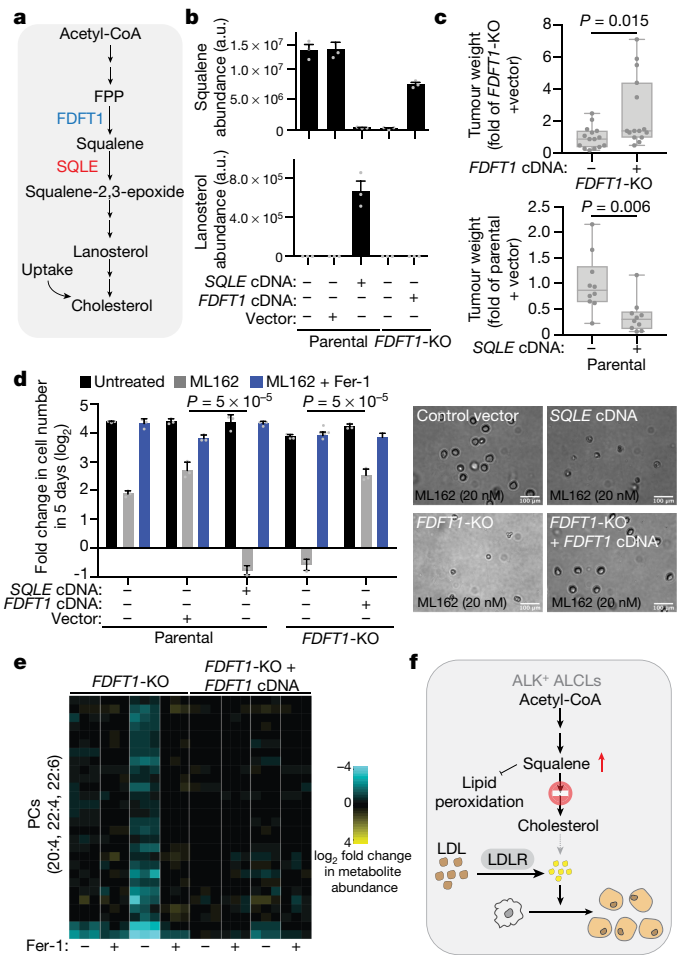


Fig. 4 | Squalene accumulation rewires membrane lipid composition and protects ALCLs from ferroptosis. **a**, Metabolic reactions catalysed by FDFT1 and SQLE in the cholesterol synthesis pathway. **b**, Squalene and lanosterol abundance in indicated Karpas299 cell lines. **c**, Relative fold change in tumour weight of indicated Karpas299-derived xenografts. **d**, Relative fold change in cell viability of indicated Karpas299 cells in the absence and presence of ML162 (20 nM) and ferrostatin-1 (Fer-1, 1 μ M) for 5 days (left). Representative bright-field micrographs of indicated Karpas299 cells after treatment (right). **e**, Heat map showing fold changes (\log_2) in PUFA-containing phosphatidylcholines (PCs) of indicated Karpas299 cell lines after incubation with Fer-1 (1 μ M) and ML162 (200 nM) for 24 h. **f**, Model depicting how loss of SQLE expression results in cholesterol auxotrophy and the accumulation of squalene in ALCLs. Excess squalene may in turn protect ALCLs from lipid peroxidation damage. **b, d**, Bars represent mean \pm s.d.; **c**, boxes represent the median, and the first and third quartiles, and the whiskers represent the minimum and maximum of all data points. **b, d**, n = 3 biologically independent samples; **c**, n = 10–15 biologically independent samples. Statistical significance was determined by two-tailed unpaired t-test.

ALCL tumours in our pre-clinical PDX models, inhibitors of *LDLR* or approaches that decrease serum cholesterol without increasing tumour *LDLR* levels might have value in the clinic²⁸. Lastly, the workflow we describe can serve as a generalizable approach for identifying additional nutrient dependencies and pro-tumorigenic metabolites across cancer types.

Online content

Any methods, additional references, Nature Research reporting summaries, source data, statements of data availability and associated accession codes are available at <https://doi.org/10.1038/s41586-019-0945-5>.

Received: 17 December 2017; Accepted: 14 January 2019;
Published online 13 February 2019.

1. Goldstein, J. L. & Brown, M. S. Regulation of the mevalonate pathway. *Nature* **343**, 425–430 (1990).
2. Delage, B. et al. Arginine deprivation and argininosuccinate synthetase expression in the treatment of cancer. *Int. J. Cancer* **126**, 2762–2772 (2010).
3. Kidd, J. G. Regression of transplanted lymphomas induced *in vivo* by means of normal guinea pig serum. II. Studies on the nature of the active serum constituent: histological mechanism of the regression: tests for effects of guinea pig serum on lymphoma cells *in vitro*: discussion. *Nature* **98**, 583–606 (1953).
4. Letouzé, E. et al. SDH mutations establish a hypermethylator phenotype in paraganglioma. *Cancer Cell* **23**, 739–752 (2013).
5. Lu, C. & Thompson, C. B. Metabolic regulation of epigenetics. *Cell Metab.* **16**, 9–17 (2012).
6. Xu, W. et al. Oncometabolite 2-hydroxyglutarate is a competitive inhibitor of α-ketoglutarate-dependent dioxygenases. *Cancer Cell* **19**, 17–30 (2011).
7. Esfahani, M., Scerbo, L. & Devlin, T. M. A requirement for cholesterol and its structural features for a human macrophage-like cell line. *J. Cell. Biochem.* **25**, 87–97 (1984).
8. Villa, G. R. et al. An LXR–cholesterol axis creates a metabolic co-dependency for brain cancers. *Cancer Cell* **30**, 683–693 (2016).
9. Brown, M. S., Kovanen, P. T. & Goldstein, J. L. Regulation of plasma cholesterol by lipoprotein receptors. *Science* **212**, 628–635 (1981).
10. Calleros, L., Sánchez-Hernández, I., Baquero, P., Toro, M. J. & Chiloeches, A. Oncogenic Ras, but not V600E-B-RAF, protects from cholesterol depletion-induced apoptosis through the PI3K/AKT pathway in colorectal cancer cells. *Carcinogenesis* **30**, 1670–1677 (2009).
11. Gill, S., Stevenson, J., Kristiana, I. & Brown, A. J. Cholesterol-dependent degradation of squalene monooxygenase, a control point in cholesterol synthesis beyond HMG-CoA reductase. *Cell Metab.* **13**, 260–273 (2011).
12. Crescenzo, R. et al. Convergent mutations and kinase fusions lead to oncogenic STAT3 activation in anaplastic large cell lymphoma. *Cancer Cell* **27**, 516–532 (2015).
13. Sullivan, L. B., Gui, D. Y. & Vander Heiden, M. G. Altered metabolite levels in cancer: implications for tumour biology and cancer therapy. *Nat. Rev. Cancer* **16**, 680–693 (2016).
14. Finotti, E., D'Ambrosio, M., Paoletti, F., Vivanti, V. & Quaglia, G. Synergistic effects of α-tocopherol, β-sitosterol and squalene on antioxidant activity assayed by crocin bleaching method. *Nahrung* **44**, 373–374 (2000).
15. Huang, Z. R., Lin, Y. K. & Fang, J. Y. Biological and pharmacological activities of squalene and related compounds: potential uses in cosmetic dermatology. *Molecules* **14**, 540–554 (2009).
16. Dixon, S. J. et al. Ferroptosis: an iron-dependent form of nonapoptotic cell death. *Cell* **149**, 1060–1072 (2012).
17. Friedmann Angeli, J. P. et al. Inactivation of the ferroptosis regulator Gpx4 triggers acute renal failure in mice. *Nat. Cell Biol.* **16**, 1180–1191 (2014).
18. Yang, W. S. et al. Regulation of ferroptotic cancer cell death by GPX4. *Cell* **156**, 317–331 (2014).
19. Kagan, V. E. et al. Oxidized arachidonic and adrenic PEs navigate cells to ferroptosis. *Nat. Chem. Biol.* **13**, 81–90 (2017).
20. Shimada, K. et al. Global survey of cell death mechanisms reveals metabolic regulation of ferroptosis. *Nat. Chem. Biol.* **12**, 497–503 (2016).
21. Viswanathan, V. S. et al. Dependency of a therapy-resistant state of cancer cells on a lipid peroxidase pathway. *Nature* **547**, 453–457 (2017).
22. Isaacs, J. S. et al. HIF overexpression correlates with biallelic loss of fumarate hydratase in renal cancer: novel role of fumarate in regulation of HIF stability. *Cancer Cell* **8**, 143–153 (2005).
23. Pollard, P. J. et al. Targeted inactivation of fh1 causes proliferative renal cyst development and activation of the hypoxia pathway. *Cancer Cell* **11**, 311–319 (2007).
24. Romero, R. et al. Keap1 loss promotes Kras-driven lung cancer and results in dependence on glutaminolysis. *Nat. Med.* **23**, 1362–1368 (2017).
25. Hangauer, M. J. et al. Drug-tolerant persister cancer cells are vulnerable to GPX4 inhibition. *Nature* **551**, 247–250 (2017).
26. Piskounova, E. et al. Oxidative stress inhibits distant metastasis by human melanoma cells. *Nature* **527**, 186–191 (2015).
27. Alvarez, S. W. et al. NFS1 undergoes positive selection in lung tumours and protects cells from ferroptosis. *Nature* **551**, 639–643 (2017).
28. Gambacorti Passerini, C. et al. Crizotinib in advanced, chemoresistant anaplastic lymphoma kinase-positive lymphoma patients. *J. Natl. Cancer Inst.* **106**, djt378 (2014).

Acknowledgements We thank all members of the Birsoy laboratory for helpful suggestions. We also thank R. Sordella for DD-Cas9 lentiviral plasmid, and R. Milne and J. Ersching for LDLR hybridoma cells. This research was supported by an EMBO long-term fellowship (EMBO ALTF 887–2016) to J.G.-B.; and by grants from the NIH (R01 CA103866 and R37 AI47389) and Department of Defense (W81XWH-07-0448) to D.M.S. AIRC Special Program in Clinical Molecular Oncology (10007), SCOR LLS and the Sandra and Edward Meyer Cancer Center PDTX Shared Resource supported G.I. D.M.S is an investigator of the HHMI and ACS Research Professor. K.B. was supported by K22 (1K22CA193660), DP2 (DP2 CA228042-01), Irma-Hirsch Trust Scholarship, Chapman-Perelman MMRF grant, AACR NextGen Grant, and is a Pew-Stewart, Searle, Sidney Kimmel and Basil O'Connor Scholar.

Reviewer information *Nature* thanks M. Conrad and the other anonymous reviewer(s) for their contribution to the peer review of this work.

Author contributions K.B. and J.G.-B. conceived the project and designed the experiments. J.G.-B. performed most of the experiments with help from L.B. and R.G. L.B. performed CRISPR screens. L.B. and B.T. assisted with tumour xenograft experiments. E.C.B. and B.Y. performed cell competition experiments. K.L. performed computational analysis. Y.S. and W.M. designed SRS chemical imaging and generated images. G.I. and D.F. provided primary and patient-derived tumour models and performed immunohistochemistry. S.H.C., C.L. and E.F. performed lipidomics. K.B. and J.G.-B. wrote the manuscript with edits from D.M.S.

Competing interests The authors declare no competing interests.

Additional information

Extended data is available for this paper at <https://doi.org/10.1038/s41586-019-0945-5>.

Supplementary information is available for this paper at <https://doi.org/10.1038/s41586-019-0945-5>.

Reprints and permissions information is available at <http://www.nature.com/reprints>.

Correspondence and requests for materials should be addressed to K.B.

Publisher's note: Springer Nature remains neutral with regard to jurisdictional claims in published maps and institutional affiliations.

© The Author(s), under exclusive licence to Springer Nature Limited 2019

METHODS

Data reporting. No statistical methods were used to predetermine sample size. **Cell lines, compounds and constructs.** Antibodies to SQLE were purchased from ProteinTech (12544-1-AP; immunoblotting) and Atlas Antibodies (HPA020762; immunohistochemistry). Beta-actin (GTX109639), ACSL4 (GTX100260) and GAPDH (GTX627408) antibodies were obtained from GeneTex; LDL receptor (ab52818), NPC1 (ab36983) and GPX4 (ab41787) antibodies from Abcam; FDFT1 antibody from Protein Tech (13128-1-AP); and ALK (C26G7), STAT3 (9132), phospho-STAT3 (9131) and Histone H3 (4499) antibodies from CST.

Horseradish peroxidase (HRP)-conjugated anti-rabbit antibody was purchased from Santa Cruz; mouse IgG1 isotype control antibody from BioCell; Matrigel from Corning; fetal bovine serum, polybrene, puromycin, squalene and cholesterol from Sigma; blasticidin from Invivogen; LDL from Lee BioSolutions; oleic acid from Santa Cruz; and Dil-LDL, DAPI and BODIPY 581/591 C11 from Thermo Fisher Scientific.

NB-598 Maleate (SQLE inhibitor, SQLEi) was obtained from Adooq Bioscience; ML162 from Aobious; erastin from Tocris; RSL3 from Selleckchem; zaragozic acid A (ZA) from Cayman Chemical; Ferrostatin-1 from Abcam; 4-nitrobenzoate (4-NB) from Alfa Aesar; crizotinib, atorvastatin, 5-azacytidine and 5-Aza-2'-deoxycytidine (Decitabine) from Sigma; and Shield-1 from CheminPharma.

Cell culture images were taken with a REVOLVE4 microscope (Echo Laboratories).

All cell lines used in this study were purchased from ATCC and DSMZ or a gift of Sabatini and Weinberg labs. The identities of all the cell lines used in this study were authenticated by single tandem repeat profiling. All the cell lines were routinely tested for mycoplasma contamination every two months. Among all the cell lines, two of them were in ICLAC as misidentified cell lines but included in our analysis for diversity owing to their oncogene status and metabolic phenotypes: U-937 is a rare histiocytic lymphoma cell line described as auxotrophic for cholesterol, and NCI-H929 is a myeloma cell line with low GLUT3 expression.

All cell lines were cultured in RPMI medium (Gibco) containing 1 mM glutamine, 10% fetal bovine serum, penicillin and streptomycin. For proliferation experiments in the absence of serum lipoproteins, regular RPMI was supplemented with 10% fetal bovine lipoprotein deficient serum (LPDS), obtained from Kalen Biomedical. For tracing experiments, [$^{\text{U}}\text{-}{}^{13}\text{C}$]sodium acetate (Cambridge Isotope Laboratories, CLM-156) was used.

For generation of the lentiviral knockout constructs, annealed oligonucleotides (below) were cloned into lentiCRISPR-v2 vector or an inducible DD-Cas9 lentiviral plasmid²⁹ using a T4 ligase (NEB). sgACSL4_3 forward, 5'-CACCGAA TGACAAGCCAAACCCAG-3'; sgACSL4_3 reverse, 5'-AAACCTGGGGTT TGGCTTGTCAATT-3'; sgCTRL_1 forward, 5'-CACCGAACGTTGGCACT ACTTCAC-3'; sgCTRL_1 reverse, 5'-AAACGTGAAGTAGTGCAACGTT-3'; sgCTRL_2 forward, 5'-CACCGTGTGCCTCCGGCGTA-3'; sgCTRL_2 reverse, 5'-AAACTACCGCCGGAAGCGCACGAC-3'; sgCTRL_3 forward, 5'-CACCGTGCCGAGTAATAACGCGAG-3'; sgCTRL_3 reverse, 5'-AACCTCGCGTTATTACTCGGCAC-3'; sgCTRL_4 forward, 5'-CACCGTAGGACCTCACGGCGCG-3'; sgCTRL_4 reverse, 5'-AAAC GCGCGCCGTGAGGTCTTAC-3'; sgCTRL_5 forward, 5'-CACCGCGGATT AGAGGTAATCGGG-3'; sgCTRL_5 reverse, 5'-AAACCCGATTACCTCT TAATCCGC-3'; sgLDLR_2 forward, 5'-CACCGTAGAAGAGAGGTAG GCGA-3'; sgLDLR_2R, 5'-AAACTCGCCTACCTCTTCTCACC-3'; sgLDLR_3F, 5'-CACCGCTGCGAGCATGGGCCCTG-3'; sgLDLR_3 reverse, 5'-AAACCAGGGCCCCATGCTCGCAGC-3'; sgLDLR_4 forward, 5'-CACCGCCTGGGCTGAAATTGCGC-3'; sgLDLR_4 reverse, 5'-AAACGCGCAATTCCAGCCCCAGGC-3'; sgLDLR_5 forward, 5'-CACCGTGGCCCAGCGAAGATGCGA-3'; sgLDLR_5 reverse, 5'-AAACTCGCATCTCGCTGGGCCAC-3'; sgFDFT1_3 forward, 5'-CACCGGTCTGGAGGACTTCCCAA-3'; sgFDFT1_3 reverse, 5'-AAACTTGGGAAGTCTCCAGCACC-3'; sgFDFT1_5 forward, 5'-CACCGCGGGAGAATGGCATTGGGA-3'; sgFDFT1_5 reverse, 5'-AAACTCCAATGCCATTCTCCGGC-3'; sgFDFT1_7 forward, 5'-CACCGCGGAAGGTGATGCCAAGA-3'; sgFDFT1_7 reverse, 5'-AAACTCTGGGCATCACCTCCGC-3'; sgFDFT1_8 forward, 5'-CACCGTTCATGGAGAGCAAGGAGA-3'; sgFDFT1_8 reverse, 5'-AAACTCTCCTGCTCTCCATGAAC-3'; sgFDFT1_10 forward, 5'-CACCGACTATCTGGAAGACCAGCA-3'; sgFDFT1_10 reverse, 5'-AAACTGCTGGTCTCCAGATAAGTC-3'; sgAAVS1 forward, 5'-CACCGGGGCCACTAGGGACAGGAT-3'; sgAAVS1 reverse, 5'-AACATCCTGCTCCATTGGGCC-3'; sgSQLE_5 forward, 5'-CACCGCAGCTGTGCTTCCAGAGA-3'; sgSQLE_5 reverse, 5'-AAACTCTGGAAAGCACAGCTGC-3'.

SQLE cDNA and sgRNA-resistant FDFT1 cDNA were synthesized as gBlock (IDT) and cloned into PMXS-IRES-Blast vector by Gibson assembly. HSD17B7 was cloned using the following primers: HSD17B7 forward,

5'-ATGGATCCGCCACCATGCGAAAGGTGGTTTGATCACCGG-3'; HSD17B7 reverse, 5'-ATGCCGCCGCTTATAGGCATGCCACTGAGCCTGG-3'.

Cloning of oncogenic NPM-ALK into PMXS-IRES-Blast by Gibson assembly was achieved by PCR of wild-type *NPM-ALK* (*NPM* is also known as *NPM1*) or its dead kinase version from previously generated constructs³⁰ using the following prime rs: *NPM-ALK* forward, 5'-GCCGATCTAGCTAGTTAATTAGCCACCG CCACCATGGAAGATTGATGCCACATGG-3'; *NPM-ALK* reverse, 5'-GGGC GGAATTACGTAGCTCAGGGCCCAGGCTGGTCATG-3'.

Proliferation assays. Cell lines were cultured in 96-well plates at 5,000 cells per well in a final volume of 0.2 ml RPMI-1640 medium (Gibco) with the indicated treatments. After 5 days of growth, 40 μl of Cell Titer Glo reagent (Promega) was added and luminescence was read using a SpectraMax M3 plate reader (Molecular Devices). Data are presented as relative fold change in luminescence to that of untreated cells. For proliferation assays under lipoprotein depletion, RPMI medium was supplemented with 10% LPDS and luminescence was read after 6 days of growth. Data are presented as relative fold change in luminescence to that of cells grown in LPDS medium supplemented with 100 $\mu\text{g ml}^{-1}$ LDL. In cholesterol rescue experiments, 100 $\mu\text{g ml}^{-1}$ LDL (corresponding to total 50 $\mu\text{g ml}^{-1}$ of cholesterol) or 10 $\mu\text{g ml}^{-1}$ free cholesterol were used, as higher free cholesterol levels impair viability of cell lines.

Of note, in our proliferation assays, we observed that glutamine levels—which correlate with the freshness of the culture medium—affect the dose of ML162 required to reduce cell proliferation and viability.

Real-time PCR assays. RNA was isolated by a RNeasy Kit (Qiagen) according to the manufacturer's protocol. RNA was spectrophotometrically quantified and equal amounts were used for cDNA synthesis with the Superscript II RT Kit (Invitrogen). qPCR analysis was performed on an ABI Real Time PCR System (Applied Biosystems) with the SYBR green Mastermix (Applied Biosystems). The primers used are: human SQLE forward, 5'-TCCTGCTCAGGGCTTTATG-3'; human SQLE reverse, 5'-AGGGTTAGGAGACAATACAGAAAG-3'; HSD17B7 forward, 5'-GACCTTTGAGTGTGGCTTG-3'; HSD17B7 reverse, 5'-ACCGA GGCAGAATTCCATATG-3'; RPLO forward, 5'-CCTCTTCCCTTCG GTGTG-3'; RPLO reverse, 5'-AATCTGGCATCAGGGACAC-3'; NPM forward, 5'-GGCCAGTGCATATTAGTGG-3'; ALK reverse, 5'-TGTACTCAGGGCTCT GCAGCT-3'; human β -actin forward, 5'-TTTGGCTATACCTACTGGCA-3'; human β -actin reverse, 5'-CTGCACAGTCGTCAGCATATC-3'; mouse SQLE forward, 5'-CCCAAACACAAAATCCTAG-3'; mouse SQLE reverse, 5'-GCAA TGCCAAGAAAAGTCCAC-3'; mouse β -actin forward, 5'-GTTGTGAATGT ATTGGCTCAGG-3'; mouse β -actin reverse, 5'-AATATTGAAAGCAA CCCAACAGG-3'. Results were normalized to RPLO or β -actin.

Dil-LDL uptake. Cells were washed twice in HBSS (Gibco) and resuspended (250,000 cells per replicate) in 0.5 ml of LPDS medium supplemented with 5 $\mu\text{g ml}^{-1}$ of Dil-LDL. To measure non-specific emission, one control well was used by adding 5 $\mu\text{g ml}^{-1}$ of non-fluorescent unlabelled LDL. Cells were incubated at 37 °C for 6 h before collection in 1.5 ml tubes and two consecutive washes with HBSS. Cells were then lysed with 100 μl of radioimmunoprecipitation assay (RIPA) buffer and spun down for 5 min at 20,000g. Fifty microlitres of the supernatants was transferred to a 96-well plate (Greiner) and fluorescence was measured with a SpectraMax M3 plate reader at an excitation wavelength of 520 nm and an emission wavelength of 580 nm. Dil-LDL uptake is shown as the specific Dil-LDL emission at 580 nm per μg of protein.

Generation of knockout and cDNA overexpression cell lines. For inducible knockout experiments, sgRNAs targeting *LDLR* (5'-GCTCG AGCATGGGCCCTG-3'), *ACSL4* (5'-GAATGACAAGCCAAACCCAG-3') or a control sgRNA (AAVS1, 5'-GGGGCCACTAGGGACAGGAT-3') were cloned into lentiviral DD-Cas9 vector. This vector was transfected into HEK293T cells with lentiviral packaging vectors VSV-G and Delta-VPR using XtremeGene transfection reagent (Roche). For transduction, indicated cells were spin-infected in 6-well tissue culture plates using 8 $\mu\text{g ml}^{-1}$ of polybrene at 1,200g for 1.5 h and selected by puromycin before addition of 250 nM Shield-1 reagent for 3 days. The knockout of the target gene was verified by immunoblotting. For generation of FDFT1-knockout cells or SQLE-knockout cells, an sgRNA targeting *FDFT1* (5'-GCCGAGAATGGCATTGGGA-3') or *SQLE* (5'-GCAGCTGTGCTTCCAGAGA-3') was cloned into lentiCRISPR-v2. After transduction and selection using puromycin, cells were single-cell cloned. For overexpression of SQLE, guide-resistant version of FDFT1, NPM-ALK or its dead kinase version, retroviral vectors with indicated cDNAs were transfected with retroviral packaging plasmids Gag-pol and VSV-G into HEK293T cells. After transduction, cells were selected with blasticidin.

Metabolite profiling and isotope tracing. For lipid metabolite profiling experiments, each indicated cell line (1×10^6 cells per replicate) was cultured as triplicates in 6-well plates and treated for 24 h with ML162 (200 nM), Fer-1 (1 μM), ZA (20 μM), 4-NB (1 mM) or atorvastatin (1 μM) before collection of cells and two consecutive washes with 1 ml of cold 0.9% NaCl. To measure squalene synthesis,

SNU-1 cells were seeded in 60 mm dishes at 70% confluence. After 24 h, cells were given fresh medium with [$^{\text{U}}\text{-}{}^{13}\text{C}$]sodium acetate (10 mM). Cell pellets were resuspended in 600 μl of cold LC/MS grade methanol, and non-polar metabolites extracted by consecutive addition of 300 μl LC/MS grade water followed by 400 μl of LC/MS grade chloroform. After 10 min extraction by vortexing and centrifugation for 10 min at 10,000 g and 4 °C, the lower lipid-containing layer was carefully collected and dried under nitrogen. Dried lipid extracts were stored at –80 °C until LC/MS analysis.

Lipids were separated on an Ascentis Express C18 2.1 mm \times 150 mm \times 2.7 μm column (Sigma-Aldrich) connected to a Dionex UltiMate 3000 UPLC system and a QExactive benchtop orbitrap mass spectrometer (Thermo Fisher Scientific) equipped with a heated electrospray ionization (HESI) probe. Dried lipid extracts were reconstituted in 50 μl 65:30:5 acetonitrile:isopropanol:water (v/v/v) and 5 μl of sample were injected into the LC/MS/MS, with separate injections for positive and negative ionization modes. Mobile phase A in the chromatographic method consisted of 60:40 water:acetonitrile with 10 mM ammonium formate and 0.1% formic acid, and mobile phase B consisted of 90:10 isopropanol:acetonitrile, with 10 mM ammonium formate and 0.1% formic acid. The chromatographic gradient has previously been described³¹. The column oven and autosampler were held at 55 °C and 4 °C, respectively. The mass spectrometer parameters have previously been described³². The spray voltage was set to 4.2 kV, and the heated capillary and the HESI were held at 320 °C and 300 °C, respectively. The S-lens RF level was set to 50, and the sheath and auxiliary gas were set to 35 and 3 units, respectively. These conditions were held constant for both positive and negative ionization mode acquisitions. External mass calibration was performed every seven days using the standard calibration mixture.

Mass spectra were acquired in both full-scan and data-dependent MS/MS mode. For the full-scan acquisition, the resolution was set to 70,000, the AGC target was 1×10^6 , the maximum injection time was 50 ms, and the scan range was $m/z = 133.4 - 2,000$. For data-dependent MS/MS, the top 10 ions in each full scan were isolated with a 1.0 Da window, fragmented with a step-wise collision energy of 15, 25 and 35 units, and analysed at a resolution of 17,500 with an AGC target of 2×10^5 and a maximum injection time of 100 ms. The underfill ratio was set to 0. The selection of the top 10 ions was set to isotopic exclusion, a dynamic exclusion window of 5.0 s, and an exclusion list of background ions based on a solvent bank.

High-throughput identification and relative quantification of lipids was performed separately for positive and negative ionization mode data, using LipidSearch software (Thermo Fisher Scientific/Mitsui Knowledge Industries)^{33,34} and the default parameters for QExactive product search and alignment. After alignment, raw peak areas for all identified lipids were exported to Microsoft Excel and filtered according to the following predetermined quality control criteria: Rej ('Reject' parameter calculated by LipidSearch) equal to 0; PQ ('Peak Quality' parameter calculated by LipidSearch software) greater than 0.85; CV (standard deviation/mean peak area across triplicate injections of a represented (pooled) biological sample) below 0.4; R (linear correlation across a three-point dilution series of the representative (pooled) biological sample) greater than 0.9. Typically, approximately 70% of identified lipids passed all four quality control criteria. Raw peak areas of the filtered lipids were added together to create a total lipid signal for each sample, and individual lipid peak areas were normalized to this total signal as a control for lipid extraction and efficiency, as well as sample loading. Of note, in the total lipid quantification of FDFT1 knockout Karpas299 cells compared to rescued control, we observed an enrichment of membrane phospholipids containing saturated fatty acids (Extended Data Fig. 7c), probably due to the fact that these species are more resistant to oxidative stress and may replace or be enriched in membrane lipids upon oxidative stress.

To measure cholesterol, lanosterol, squalene and CoQ10, a XCalibur QuanBrowser 2.2 (Thermo Fisher Scientific) was used a 5-ppm mass tolerance and referenced an in-house library of chemical standards. Total lipid signal calculated with LipidSearch was used to normalize raw peak areas to generate relative abundance.

Immunoblotting. Cell pellets were washed twice with ice-cold PBS before lysis in lysis buffer (10 mM Tris-Cl pH 7.5, 150 NaCl, 1 mM EDTA, 1% Triton X-100, 2% SDS, CHAPS 0.1%) supplemented with protease inhibitors and PhosSTOP (Roche). Each cell lysate was sonicated and, after centrifugation for 10 min at 4 °C and 20,000 g, supernatants were collected and their protein concentration determined by a Pierce BCA Protein Assay Kit (Thermo Scientific) with bovine serum albumin as a protein standard. Samples were resolved on 8% or 12% SDS-PAGE gels and analysed by immunoblotting as previously described³⁵.

Targeted bisulfite sequencing. Assays were designed targeting CpG sites in SQLE promoter region using primers created with Rosefinch. All primers were resuspended in TE solution at 100 μM and validated using 1 ng of bisulfite-converted control DNA. Following primer validation, samples were bisulfite converted using the EZ DNA Methylation-Lightning Kit (Zymo D5030) according to the manufacturer's instructions. Multiplex amplification of all samples with specific primer

pairs and the Fluidigm Access Array System was performed according to the manufacturer's instructions. The resulting amplicons were pooled for collection and subsequent barcoding according to the Fluidigm instrument's guidelines. After barcoding, samples were purified by a ZR-96 DNA Clean & Concentrator (Zymo D4023) and then prepared for massively parallel sequencing using a MiSeq V2 300 bp Reagent Kit and paired-end sequencing protocol according to the manufacturer's guidelines.

Sequence reads were identified by a standard Illumina base-calling software and then analysed by a Zymo Research proprietary analysis pipeline, which is written in Python. Low-quality nucleotides and adaptor sequences were trimmed off during analysis quality control. Sequence reads were aligned back to the reference genome using Bismark, an aligner optimized for bisulfite sequence data and methylation calling³⁶. Paired-end alignment was used as default thus requiring both read 1 and read 2 be aligned within a certain distance, otherwise both read 1 and read 2 were discarded. Index files were constructed using the 'bismark_genome_preparation' command and the entire reference genome. The '-non_directional' parameter was applied while running Bismark. All other parameters were set to default. Nucleotides in primers were trimmed off from amplicons during methylation calling. The methylation level of each sampled cytosine was estimated as the number of reads reporting a C, divided by the total number of reads reporting a C or T.

DNA barcode cell mixing. DNA barcode cell competition assay was performed as previously described using the same primer and barcoding sequences³⁵ (Supplementary Table 1). In brief, a unique 7-bp sequence was transduced into 28 different cancer cell lines using lentiviruses produced from a PLKO.1P vector. Each cell line was infected with three barcodes in separate infections for statistical analysis. To perform cell competition assays, barcoded cell lines were mixed in equal amounts and the mixed population was cultured under indicated conditions for 15 days. Cells were then collected for genomic DNA and processed for Illumina deep sequencing. Barcode abundance was determined in the starting population and after the growth.

CRISPR-based screen. The highly focused metabolism sgRNA library was designed as previously described by including representation of key genes of every mammalian metabolic pathway (Supplementary Table 3). Oligonucleotides for sgRNAs were synthesized by Integrated DNA Technologies and annealed before they were introduced in lentiCRISPR-v2 vector using a T4 DNA ligase kit (NEB), following manufacturer's instructions. Ligation products were then transformed in NEB stable competent *E. coli* (NEB) and the resulting colonies were grown overnight at 32 °C and plasmids isolated by Miniprep (QIAGEN). This plasmid pool was used to generate a lentiviral library containing five sgRNAs per gene target. This viral supernatant was titred in each cell line by infecting target cells at increasing amounts of virus in the presence of polybrene (8 $\mu\text{g ml}^{-1}$) and by determination of cell survival after 3 days of selection with puromycin. Two million of each cell type were infected at a MOI of 1 before selection with puromycin for 3 days. An initial pool of two million cells was collected. Infected cells were then cultured for 14 population doublings, after which two million cells were collected and their genomic DNA extracted by a DNeasy Blood & Tissue kit (QIAGEN). For amplification of sgRNA inserts, we performed PCR using specific primers for each condition. PCR amplicons were then purified and sequenced on a NextSeq 500 (Illumina). Sequencing reads were mapped and the abundance of each sgRNA was measured. Gene score is defined as the median \log_2 fold change in the abundance between the initial and final population of all sgRNAs targeting a particular gene.

Immunohistochemistry. Immunohistochemistry staining was performed as previously described¹². SQLE protein expression was evaluated in primary and patient-derived tumour xenograft ALCL formalin-fixed tissues samples using a rabbit polyclonal anti-human SQLE (Atlas Antibodies, 1:200).

LDLR monoclonal antibody purification. Hybridoma cell lines producing a monoclonal antibody against LDLR have previously been described³⁷. These cell lines were cultured in RPMI supplemented with 20% FBS and 2 mM pyruvate. LDLR antibody was then purified using a Protein G resin (GenScript) and Protein G Sepharose 4 Fast Flow (GE Healthcare) following the manufacturer's instructions.

C11-BODIPY lipid peroxidation. Cells were plated (250,000 cells per well) in six-well plates and treated with ML162 for 18 h before two washes with HBSS and incubation of cells in 500 μl of HBSS containing BODIPY 581/591 C11 (1 μM). After 15 min incubation at 37 °C, cells were washed twice on ice-cold HBSS and resuspended in 0.5 ml of HBSS containing 50 ng ml^{-1} DAPI and filtered into FACS tubes with cell-strainer cap (Falcon). Flow cytometry data were collected on a BD LSR II Flow Cytometer (BD Biosciences) by using an excitation wavelength of 488 nm and the FL1 collection channel. FlowJo v.10 software was used for data analysis. Live cells were selected from the starting cell population on a DAPI/FSC-A plot. Then, single cells were selected using a FSC-A/FSC-H plot from the population of live cells. Data represents populations of live singlet cells.

Spontaneous Raman spectroscopy and SRS microscopy. Spontaneous Raman spectra were acquired by a confocal Raman microspectroscopy (Xplora; HORIBA Jobin Yvon) equipped with a 532-nm (40-mW) laser and a 100 \times objective

(air, N.A. = 0.9, MPlan N; Olympus). Spectra of pure squalene and cholesterol were acquired with 5 s integration. Cell spectra were obtained from the lipid droplets (identified under bright field) of cells fixed with 4% paraformaldehyde after 120-s integration. Glass and solution background was subtracted by measuring signal from adjacent area.

Chemical imaging by SRS microscopy was acquired on an integrated inverted confocal laser-scanning microscope (FV1200; Olympus) equipped with a water-immersion 25 \times objective (1.05 N.A. XLPLNXWMP2; Olympus). Concentration mapping of selected chemical bond vibration was achieved by raster-scanning two spatially and temporally overlapped picosecond laser beams (picoEmerald, Applied Physics and Electronics) across the sample. SRS signal was generated when the frequency difference of the two beams (pump, tunable; Stokes, 1,064 nm) matched the vibrational frequency, and was subsequently extracted through high-frequency modulation transfer scheme. Specifically, the Stokes beam was modulated by an electro-optic modulator at 8MHz. Transmitted light was collected by an oil-immersion condenser (1.4 N.A.; Olympus) and filtered by a bandpass filter (890/220 CARS; Chroma Technology), so that only pump beam was detected by a Si photodiode (FDS1010; Thorlabs, biased at 64V). The terminated signal was then pre-filtered (8MHz \pm 1MHz, KR 2724; KR electronics), and then demodulated by a lock-in amplifier (SR844; Stanford Research Systems). Laser powers on sample were measured to be 120 mW (Stokes) and 100 mW (pump). Images were acquired at a speed of 100 s per pixel by Fluoview Software.

Images at three channels were obtained for each cell. The corresponding wavelengths of pump were: 928.4 nm (1,372 cm $^{-1}$), 927.2 nm (1,386 cm $^{-1}$), 926.0 nm (1,400 cm $^{-1}$). Among these, 1,386 cm $^{-1}$ is the squalene on-resonance frequency (vibrational peak), whereas 1,372 cm $^{-1}$ and 1,400 cm $^{-1}$ are the squalene off-resonance frequencies (baseline of cell mass). Thus, the image of squalene distribution is calculated as

$$I_{\text{squalene}} = I_{1386} - (I_{1372} + I_{1400})/2$$

in which I represents SRS intensity from each channel. Images were calculated (in unit of demodulated terminated photocurrent) and later assigned pseudo-colours in ImageJ.

SRS signal is proportional to concentration and it is limited by laser shot noise, thus the detection limit is usually submillimolar to millimolar³⁸. Squalene accumulates at these high concentrations in lipid droplets, and may still be present in other subcellular compartments and membranes at lower concentrations, but remains undetected by SRS microscopy.

Gene correlation of primary ALCLs and cancer cell lines. RNA-sequencing data was obtained from a previously published work with SRA accession number SRA176318¹². Differentially expressed transcripts were identified using the R package limma. False discovery rate was used to correct for multiple hypothesis testing with a significance threshold of 0.01. The identification of most differentially expressed genes was performed using Student's *t*-test statistic (Supplementary Table 2). Microarray expression data of SQLE was obtained from Cancer Cell Line Encyclopedia³⁹.

Generation of patient-derived tumour xenografts. PDX models were generated as previously described^{12,40}. In brief, tumour graft samples were cut into multiple 3 \times 3 \times 1-mm pieces (multiple pieces per specimen) in complete medium and implanted fresh and/or cryopreserved in 10% DMSO-RPMI-1640 frozen medium supplemented with 20% FCS. Six-to-eight-week-old NOD.Cg B2m^{tm1Unc} Prkdc^{scid} Il2rg^{tm1Wjl}/SzJ mice (NSG) were first anaesthetized (Rompun 0.05 μ l g $^{-1}$ Zoletil 1.6 μ g g $^{-1}$ i.m.). Then, with animals lying on their ventral site, the dorsal region was sterilized (70% ethanol). Multiple tumour-graft tissue fragments (2–4) were subcutaneously injected using a trocar. Implant growth was assessed by palpation and/or MRI scanning and collected when tumour masses were required. Tumour volumes were assessed using an electronic caliper. Recipient animals were checked regularly and killed at early sign of distress. At collection, mice were killed in a CO₂ chamber and grafts were collected for histologic evaluation, re-grafting, or snap-freezing in liquid nitrogen. Tumours were then dissociated to single cells using a phosphate buffer containing Collagenase A (25,000 U ml $^{-1}$), Dispase II (12.5 U ml $^{-1}$), DNase (500 U ml $^{-1}$). Cells were then filtered through a 100- μ m filter and washed twice in PBS. After an overnight culture in RPMI (Lonza), floating live cells were selected with a ficoll (Ficoll-Paque-Plus, GE Healthcare). Multi-colour flow cytometry was used to check the percentage of the neoplastic T cells.

Fresh and/or viable cryopreserved samples were obtained at the time of diagnosis, prior treatment or at relapse after single or multiple chemotherapy protocols. Informed consent was obtained following the procedures approved by the Weill Cornell and Memorial Sloan Cancer Center ethical committees. Diagnoses were assigned according to the WHO classification by at least two experienced pathologists. Samples IL69 and IL79 (ALK $^+$ PDX1 and ALK $^+$ PDX3 in Fig. 3h) correspond to patients who experienced a refractory clinical course unresponsive to standard

chemo-immunotherapy. Patient IL69 corresponds to a 20-year-old male patient diagnosed with ALK $^+$ ALCL and received two cycles of CHOP followed by two additional three cycles of BV-CHP. On progressive disease, the patient was treated with Crizotinib but he died with active systemic disease and CNS involvement after a month. IL79 was a 65-year-old male patient with a relapsed ALK $^+$ ALCL treated with BV-CHOP versus CHOP, who also died with progressive disease after four months of therapy (Supplementary Table 5).

Mini competition assay. Five control sgRNAs targeting intergenic regions, four sgRNAs targeting *LDLR*, and five sgRNAs targeting *FDFT1* were cloned into linearized lentiCRISPR-v2 vector and transformed in NEB competent *E. coli*. Each plasmid was then pooled at equal concentrations and used for lentivirus production as previously described. DEL cell line was infected and selected with puromycin for three days before being in vitro cultured or injected subcutaneously in NSG mice. Similarly, collagenase-digested ALCL PDX cells were transduced with the same lentiviral particles and subsequently injected subcutaneously in immunodeficient mice 24 h after infection. No antibiotic selection was performed as these cells cannot grow under standard culture conditions. Tumours were collected after 2–4 weeks of growth. An initial pool of each sample was taken for normalization. After 14–21 days guide DNAs were isolated and amplified by PCR. PCR amplicons were then sequenced on a NextSeq 500 (Illumina). Guide scores were calculated as median log₂ fold change in the abundance between the initial and final population of that sgRNA similar to standard CRISPR screens.

Mouse studies. All animal studies and procedures were conducted according to a protocol approved by the Institutional Animal Care and Use Committee (IACUC) at the Rockefeller University. All mice were maintained on a standard light-dark cycle with food and water ad libitum. For in vivo LDLR experiments, xenograft tumours were initiated by injecting 1 \times 10 6 cells per 100 μ l PBS of ALCL or control cell lines subcutaneously. For ALCL cells coming from PDXs, injections contained 1 \times 10 6 cells per 100 μ l 30% Matrigel. After injections in the left and right flanks of male and female 6–14 week-old NOD scid gamma (NSG) mice (Taconic), tumours were grown for 2–4 weeks. For patient-derived tumour xenograft models, NSG B2m and NSG mice were handled according to Weill Cornell Medical Institute's Institutional Animal Care and Use Committee-approved protocol 2014-0024. All operatively resected tumours were collected after written patient consent and in accordance with the institutional review board approved protocols of Weill Cornell Medical Institute (2014-0024, 0201005295R012, 1410015560A002 and 0107004999).

For tumour experiments with FDFT1-knockout and SQLE-expressing Karpas299 cell lines, 5–10 \times 10 4 cells per 100 μ l PBS of each cell line were injected subcutaneously into NSG mice and grown for 28 days. Injection of higher number of cells resulted in a loss of significance in tumour size difference, a result that is consistent with previously published work²⁶.

In no cases did xenograft tumour size surpassed the limit permitted by our protocol (2 cm). All treatment studies were randomized and injections were performed by blinded investigators.

Statistics and reproducibility. GraphPad PRISM 7 and Microsoft Excel 15.21.1 software were used for statistical analysis. All experiments were performed at least two times with similar results. Both technical and biological replicates were reliably reproduced.

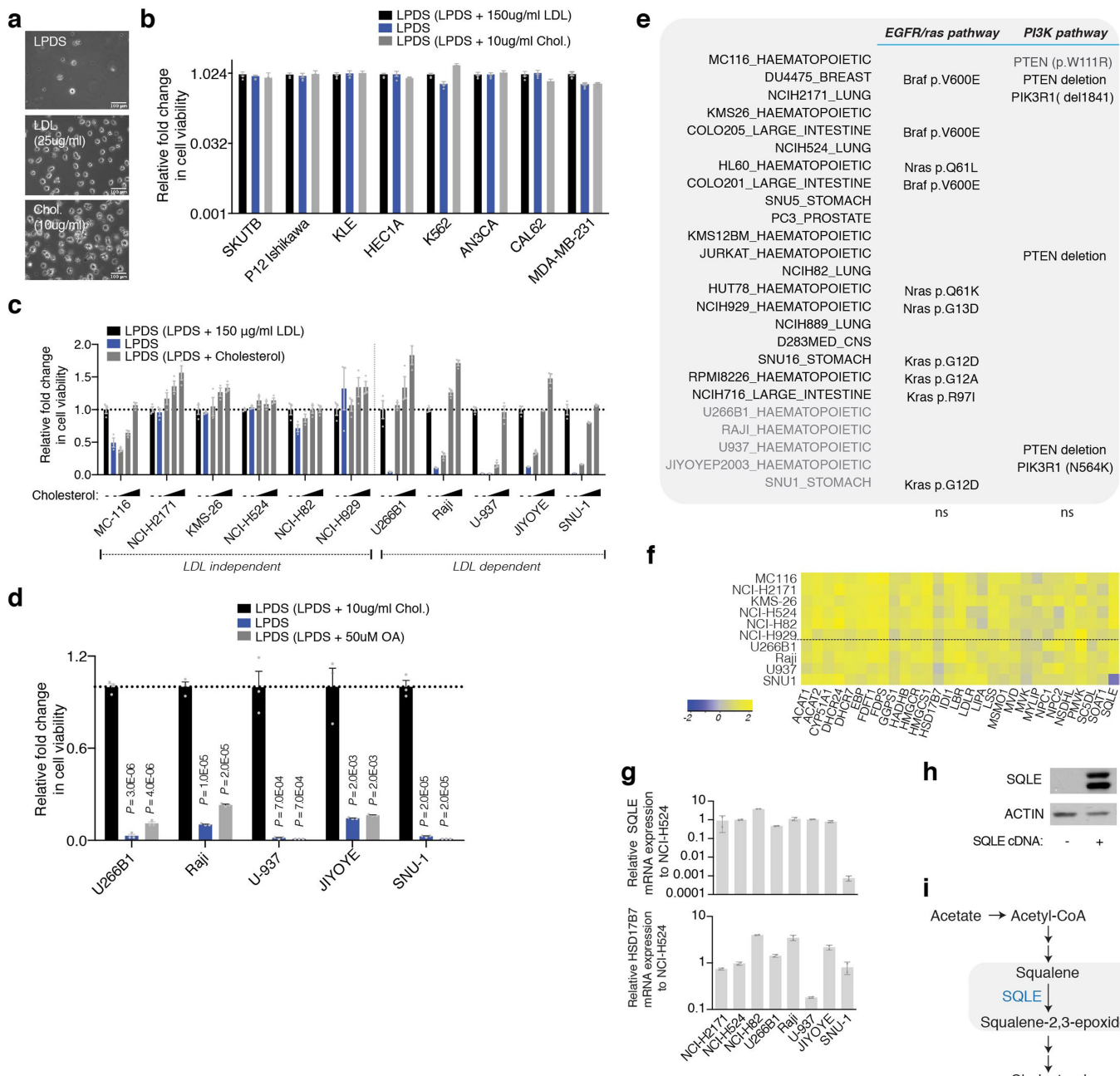
Reporting summary. Further information on research design is available in the Nature Research Reporting Summary linked to this article.

Data availability

Source data for barcoding experiment in Fig. 1 are provided as Supplementary Table 1. Gene correlation comparing RNA-sequencing data of ALK $^-$ and ALK $^+$ patients (Fig. 2i) is included in Supplementary Table 2. Gene scores of CRISPR screens in Fig. 3 and Extended Data Fig. 4 are provided as Supplementary Table 4. Clinical data of the PDXs used in Fig. 3f and Extended Data Fig. 6c are provided as Supplementary Table 5. Source Data for Figs. 1–4 and Extended Data Figs. 1–10 are available with the online version of the paper. All other data supporting the findings of this study are available from the corresponding author on reasonable request.

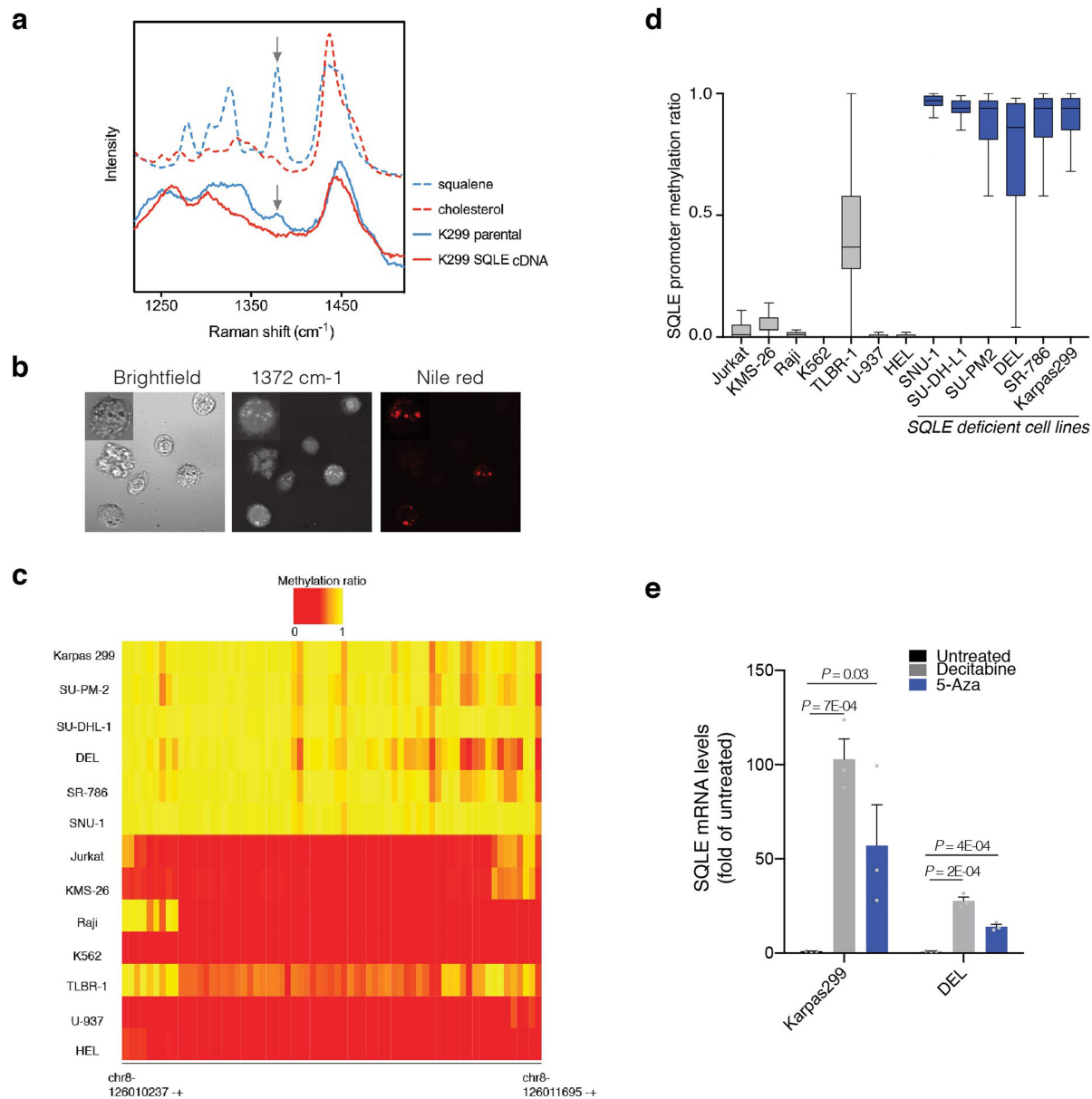
29. Senturk, S. et al. Rapid and tunable method to temporally control gene editing based on conditional Cas9 stabilization. *Nat. Commun.* **8**, 14370 (2017).
30. Ambrogio, C. et al. NPM-ALK oncogenic tyrosine kinase controls T-cell identity by transcriptional regulation and epigenetic silencing in lymphoma cells. *Cancer Res.* **69**, 8611–8619 (2009).
31. Hu, C. et al. RPLC-ion-trap-FTMS method for lipid profiling of plasma: method validation and application to p53 mutant mouse model. *J. Proteome Res.* **7**, 4982–4991 (2008).
32. Bird, S. S., Marur, V. R., Sniatynski, M. J., Greenberg, H. K. & Kristal, B. S. Serum lipidomics profiling using LC-MS and high-energy collisional dissociation fragmentation: focus on triglyceride detection and characterization. *Anal. Chem.* **83**, 6648–6657 (2011).

33. Taguchi, R. & Ishikawa, M. Precise and global identification of phospholipid molecular species by an Orbitrap mass spectrometer and automated search engine Lipid Search. *J. Chromatogr. A* **1217**, 4229–4239 (2010).
34. Yamada, T. et al. Development of a lipid profiling system using reverse-phase liquid chromatography coupled to high-resolution mass spectrometry with rapid polarity switching and an automated lipid identification software. *J. Chromatogr. A* **1292**, 211–218 (2013).
35. Birsoy, K. et al. Metabolic determinants of cancer cell sensitivity to glucose limitation and biguanides. *Nature* **508**, 108–112 (2014).
36. Krueger, F. & Andrews, S. R. Bismark: a flexible aligner and methylation caller for Bisulfite-Seq applications. *Bioinformatics* **27**, 1571–1572 (2011).
37. Nguyen, A. T., Hirama, T., Chauhan, V., Mackenzie, R. & Milne, R. Binding characteristics of a panel of monoclonal antibodies against the ligand binding domain of the human LDLr. *J. Lipid Res.* **47**, 1399–1405 (2006).
38. Freudiger, C. W. et al. Label-free biomedical imaging with high sensitivity by stimulated Raman scattering microscopy. *Science* **322**, 1857–1861 (2008).
39. Barretina, J. et al. The Cancer Cell Line Encyclopedia enables predictive modelling of anticancer drug sensitivity. *Nature* **483**, 603–607 (2012).
40. Cheng, M. et al. CEP-28122, a highly potent and selective orally active inhibitor of anaplastic lymphoma kinase with antitumor activity in experimental models of human cancers. *Mol. Cancer Ther.* **11**, 670–679 (2012).



Extended Data Fig. 1 | Extracellular cholesterol dependence of cancer cell lines. **a**, Representative bright-field micrographs of U-937 cells cultured with the indicated concentrations of cholesterol and LDL. **b**, Relative fold change in cell number of indicated cell lines cultured for five days with LPDS in the presence or absence of free cholesterol relative to LDL-replete serum. **c**, Relative fold change in cell number of indicated cell lines grown for five days under LPDS with or without free cholesterol (1, 5 or 10 $\mu\text{g ml}^{-1}$) relative to LDL-replete serum. **d**, Fold change in cell viability of cholesterol auxotrophic cancer cell lines grown for five days with LPDS in the presence or absence of cholesterol or oleic acid (OA), relative to LPDS supplemented with free cholesterol. **e**, Reported alterations in copy number or driver mutations in oncogenic EGFR/Ras and PI3K pathways of cancer cell lines used in the DNA barcode-based

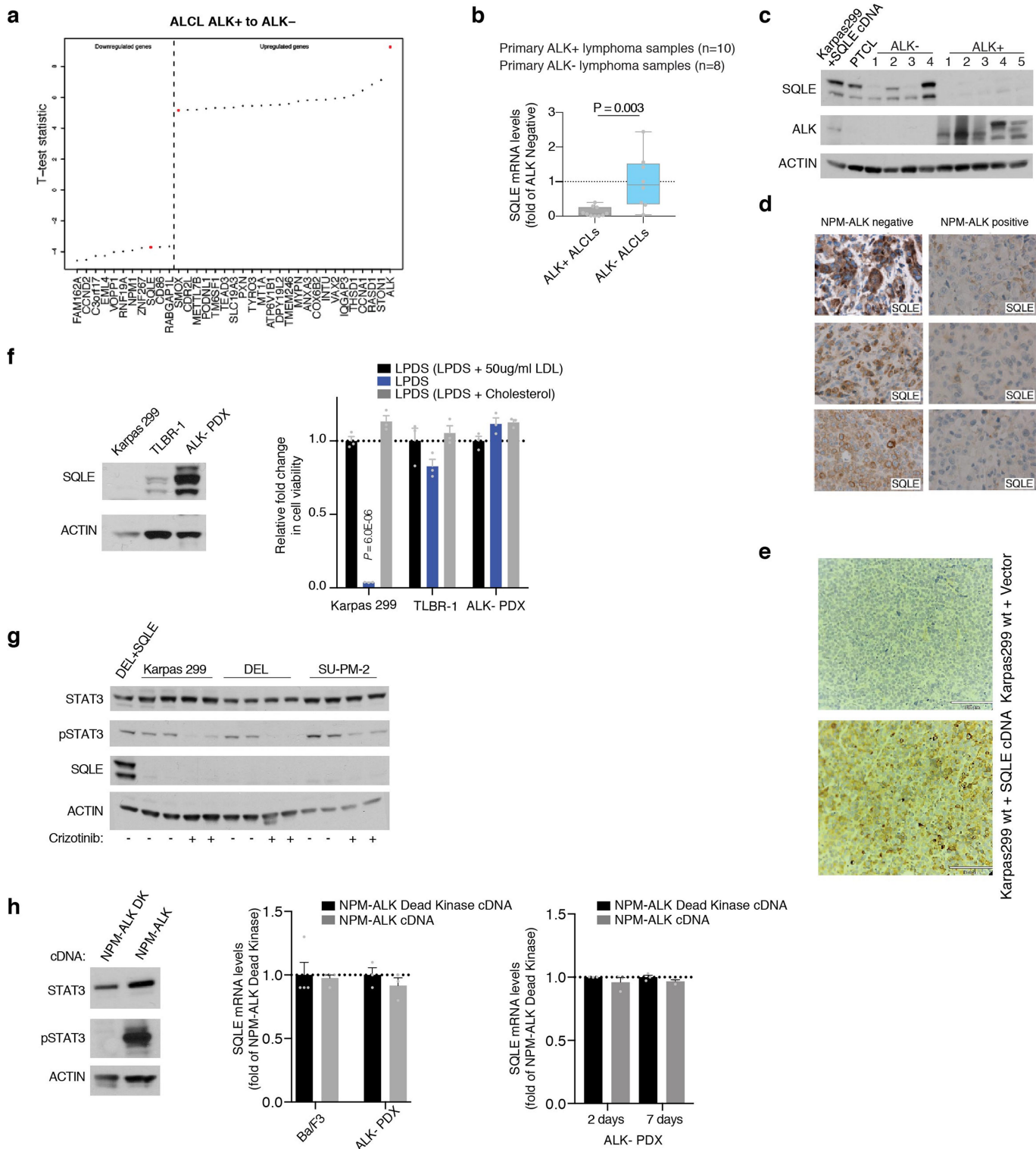
competition assay. **f**, Heat map showing mRNA expression levels of cholesterol metabolism genes in LDL-dependent and -independent cancer cell lines. Colour bar indicates scale (\log_2 transformed). **g**, SQLE and HSD17B7 mRNA levels in indicated cell lines relative to cholesterol prototroph cell line NCI-H524. mRNA levels were measured using a real-time PCR assay. RPL0 is used as a control. **h**, Immunoblotting of SQLE in SNU-1 cell lines transduced with a control vector or an SQLE cDNA. Actin is included as a loading control. **i**, Schematic depicting squalene synthesis from acetate. In **b–d** and **g**, bars represent mean \pm s.d. For **b–d**, $n = 3$ biologically independent samples. For **g**, $n = 2$ biologically independent samples. Statistical significance was measured by two-tailed unpaired t-test.



Extended Data Fig. 2 | Promoter hypermethylation of the *SQLE* gene and accumulation of squalene in lipid droplets of ALK^+ ALCs.

a, Raman spectra of squalene (blue dashed), cholesterol (red dashed) and lipid droplets in Karpas299 parental cell (blue solid), and lipid droplets in Karpas299 cell expressing *SQLE* cDNA (red solid). Lipid droplets were identified in bright field and targeted in the confocal Raman microspectrometer. Arrows indicate squalene-specific Raman peak. **b**, Representative bright-field image, SRS image obtained at cell lipid background ($1,372 \text{ cm}^{-1}$) and fluorescence of Nile Red staining (for lipid droplets) in Karpas299 cells. **c**, Heat map showing the DNA methylation ratio for the indicated genomic region containing *SQLE* promoter for

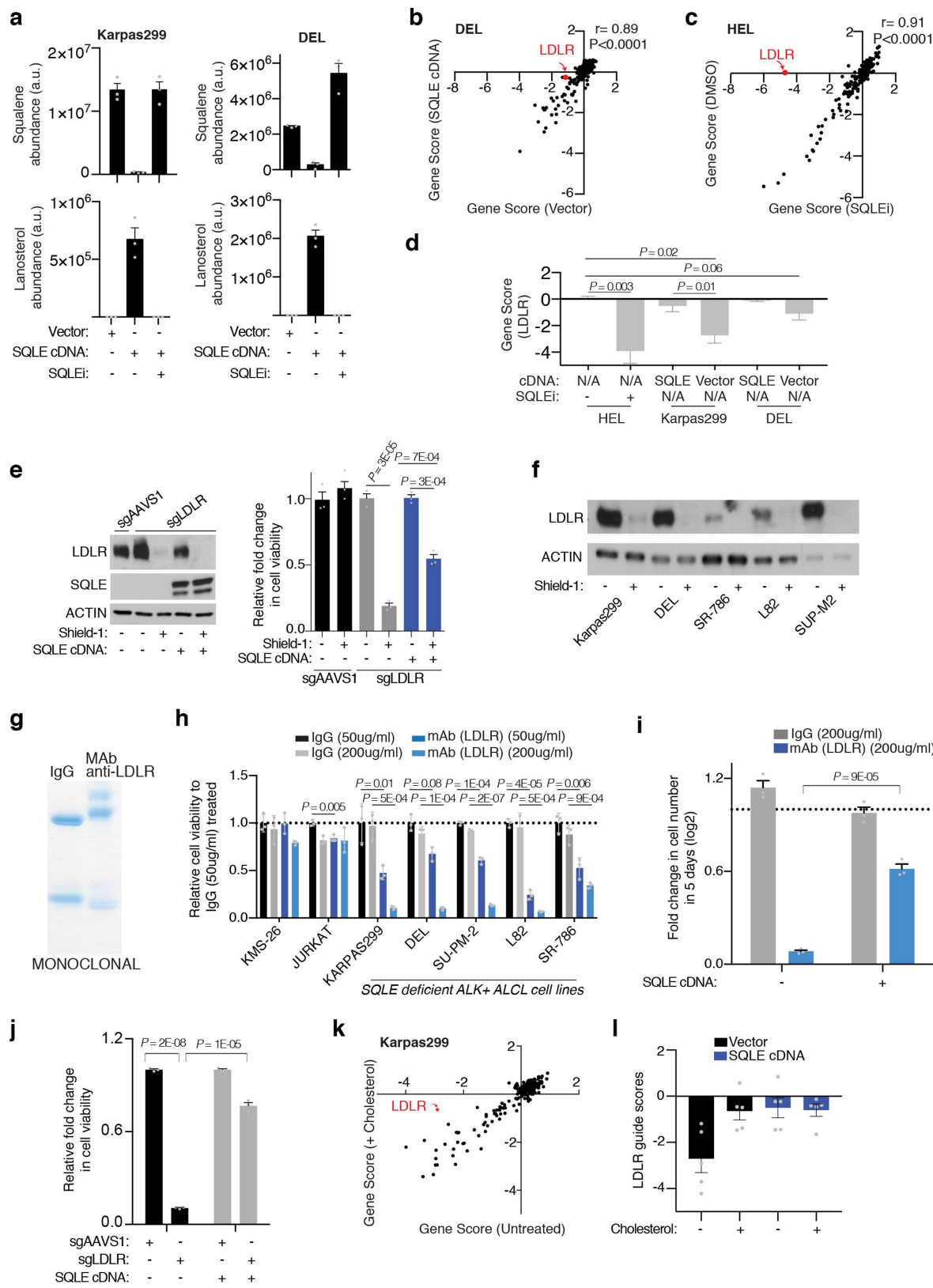
indicated cancer cell lines. Chromosomal position range and strand is indicated. Colour bar indicates scale. **d**, *SQLE* promoter methylation ratio of control (grey) and *SQLE*-deficient (blue) cancer cell lines. The boxes represent the median and the first and third quartiles, and the whiskers represent the minimum and maximum data points still within 1.5 of the interquartile range ($n = 67$ independent genomic positions per sample). **e**, Fold change in *SQLE* mRNA expression levels of indicated cell lines after treatment with decitabine (500 nM for 4 days) or 5-azacytidine (5-Aza, 1 μM for 6 days), relative to untreated cells (mean \pm s.d., $n = 3$ biologically independent samples).



Extended Data Fig. 3 | See next page for caption.

Extended Data Fig. 3 | Lack of SQLE expression in primary ALK⁺ ALCLs. **a**, List of most-upregulated and -downregulated genes from differential expression analysis of primary ALK⁺ primary samples compared to ALK⁻ samples. The student *t*-test statistic of each gene is calculated and used as a ranking metric ($n = 17$ biologically independent ALK⁻ samples, 5 biologically independent ALK⁺ samples). **b**, Fold change in *SQLE* mRNA expression levels of primary ALK⁺ ALCLs relative to primary ALK⁻ ALCLs, using actin as a control. The boxes represent the median and the first and third quartiles, and the whiskers represent the minimum and maximum of all data points. Statistical significance was determined by two-tailed unpaired *t*-test. **c**, Immunoblotting of SQLE and ALK in indicated PDX and cell line models. Actin was used as the loading control. PTCL, peripheral T cell lymphoma. **d**, Immunohistochemical staining of SQLE in ALK⁺ and ALK⁻ ALCL primary tumour samples. **e**, Immunohistochemical staining of SQLE in Karpas299 xenograft tumours transduced with a control or *SQLE* cDNA. Representative images are shown. **f**, Immunoblotting of SQLE of indicated cell lines (top). Relative fold change in cell viability of the indicated ALK⁺ (Karpas299)

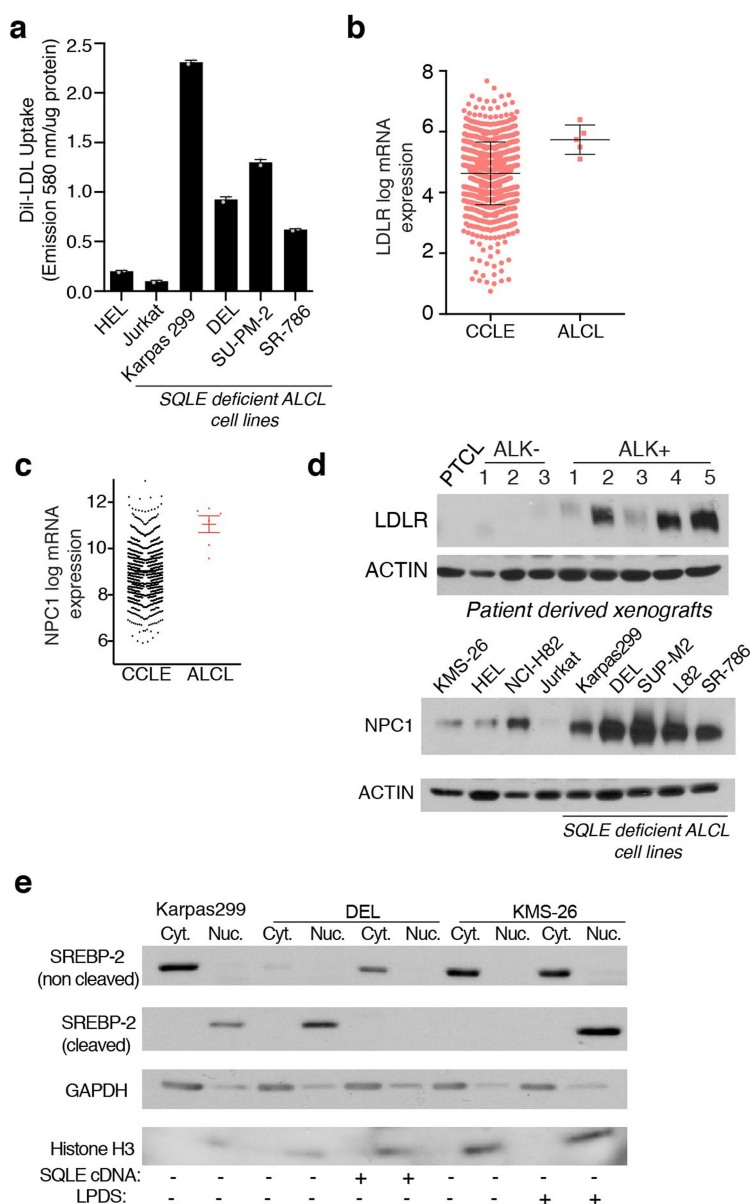
and ALK⁻ cell lines (TLBR-1 and ALK⁻ PDX cell line) grown for five days under LPDS with or without free cholesterol relative to LDL-replete serum (bottom) (mean \pm s.d., $n = 3$ biologically independent samples). **g**, Immunoblotting of STAT3, phospho-STAT3 and SQLE in indicated cell lines after 72-h treatment with crizotinib (200 nM). Actin was used as a loading control. **h**, Immunoblotting of STAT3 and phospho-STAT3 3 days after transduction of Ba/F3 with a dead kinase version of the NPM-ALK fusion (NPM-ALK DK) or with oncogenic *NPM-ALK* cDNA. **i**, *SQLE* mRNA levels of Ba/F3 and ALK⁻ ALCL cell lines two or seven days after transduction with NPM-ALK DK or NPM-ALK, relative to levels in NPM-ALK dead kinase. mRNA levels were quantified with a real-time PCR assay using β -actin as a control (mean \pm s.d., $n = 3\text{--}4$ biologically independent samples). In **b**, the boxes represent the median, and the first and third quartiles, and the whiskers represent the minimum and maximum of all data points. In **f** and **h**, bars represent mean \pm s.d. For **f** and **h**, $n = 3$ biologically independent samples. Statistical significance was determined by two-tailed unpaired *t*-test.



Extended Data Fig. 4 | See next page for caption.

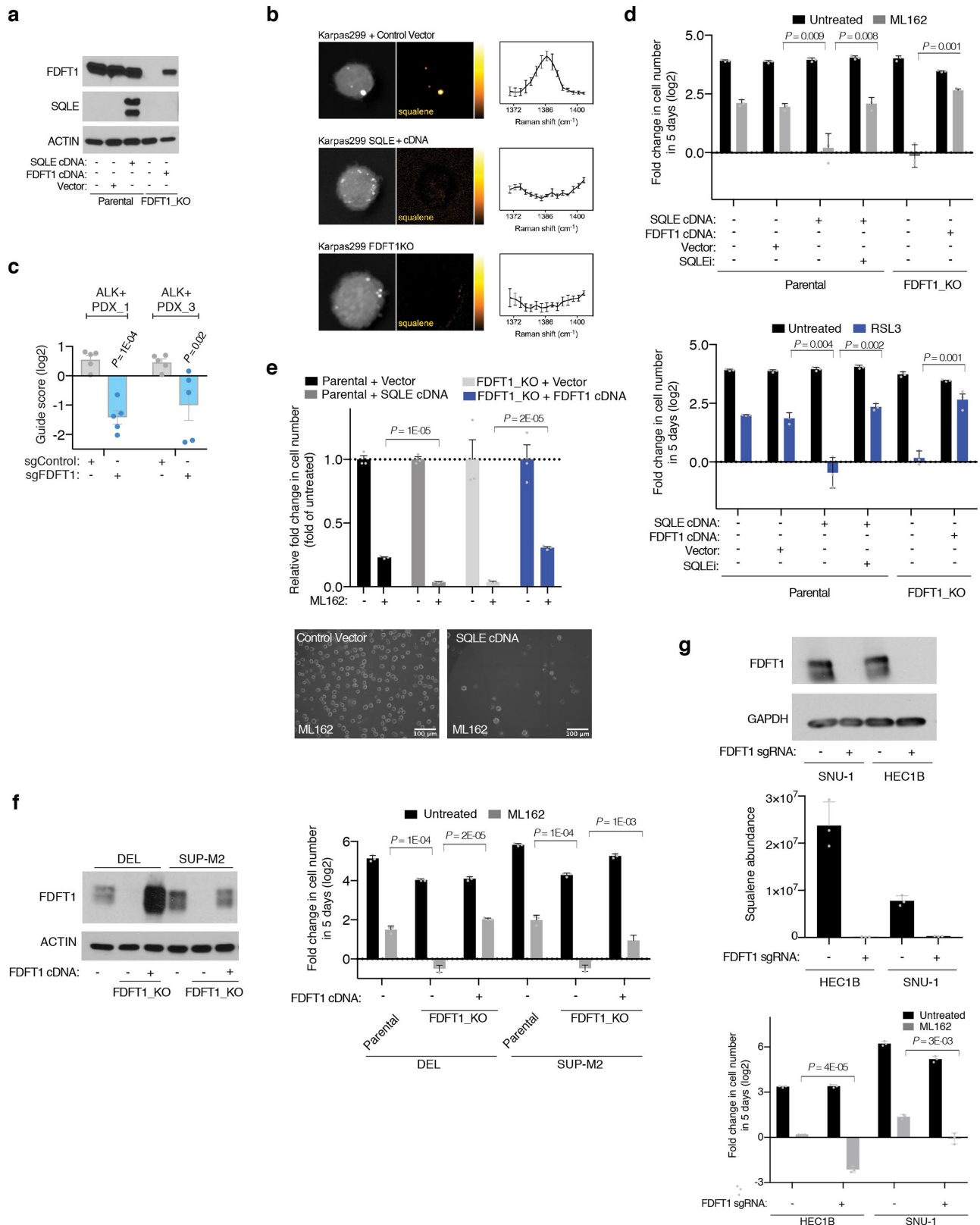
Extended Data Fig. 4 | LDLR is an essential gene for the growth of ALK⁺ ALCLs. **a**, Squalene and lanosterol abundance of Karpas299 and DEL cell lines in the absence or presence of *SQLE* cDNA or after incubation for 24 h with an SQLEi (1 μ M). **b**, Gene essentiality scores for control or *SQLE*-expressing DEL cell line. Pearson correlation coefficients are indicated. Red dot denotes LDLR. **c**, Gene essentiality scores for cholesterol-prototroph HEL cell lines in the presence or absence of an SQLEi (1 μ M). Pearson correlation coefficients are indicated. Red dot denotes LDLR. **d**, LDLR guide scores of the indicated cell lines in the presence or absence of *SQLE* inhibitor. **e**, Immunoblots for LDLR and *SQLE* in control and *SQLE*-cDNA-expressing Karpas299 cells infected with sgAAVS1 or sgLDLR virus in the presence or absence of Shield-1 (250 nM; left). Relative fold change in cell viability of indicated cancer cell lines grown in the absence and presence of Shield-1 for 5 days (right). **f**, Immunoblotting of LDLR in ALK⁺ ALCL lines transduced with an inducible sgLDLR vector in the presence or absence of Shield-1 (250 nM). Actin is used as a loading control. **g**, Relative fold change in cell viability

of control or *SQLE*-expressing DEL cell lines transduced with sgAAVS1 or sgLDLR after five days of growth. **h**, Gene essentiality scores for untreated or cholesterol-supplemented Karpas299 cell line. Red dot denotes LDLR. **i**, LDLR guide scores in Karpas299 cell lines expressing a control vector or *SQLE* cDNA in the presence or absence of cholesterol supplementation. **j**, Coomassie blue staining of control IgG and LDLR monoclonal antibodies used in proliferation assays. **k**, Relative fold change in cell viability of indicated cancer cell lines grown for five days in the presence of the indicated amounts of IgG or a monoclonal antibody against LDLR. **l**, Relative fold change in cell viability of DEL cell lines transduced with a control vector or an *SQLE* cDNA grown for five days in the presence of the indicated amounts of IgG or an anti-LDLR monoclonal antibody compared to cells grown in the absence of both. In **a**, **d**, **e**, **g**, **i**, **k** and **l** bars represent mean \pm s.d. For **a**, **e**, **g**, **i**, and **k**, $n = 3$ biologically independent samples. For **d** and **i**, $n = 5$ independent *LDLR*-targeting sgRNAs. Statistical significance was determined by two-tailed unpaired *t*-test.



Extended Data Fig. 5 | Upregulation of the LDL-cholesterol uptake pathway in ALK⁺ ALCLs. **a**, Dil-LDL uptake in the indicated cell lines. Results were normalized to protein levels (mean ± s.d., $n = 2$ biologically independent samples). **b**, mRNA expression levels of *LDLR* (log) in cell lines from CCLE database compared to that of ALK⁺ ALCL lines (mean ± s.d., $n = 1,010$ independent cell lines for CCLE collection, 5 independent cell lines for ALCL). **c**, Expression levels of Niemann-Pick C1 protein (*NPC1*) mRNA (log) in cell lines from CCLE database compared to that of ALK⁺ ALCL lines (mean ± s.d., $n = 1,010$ independent cell lines

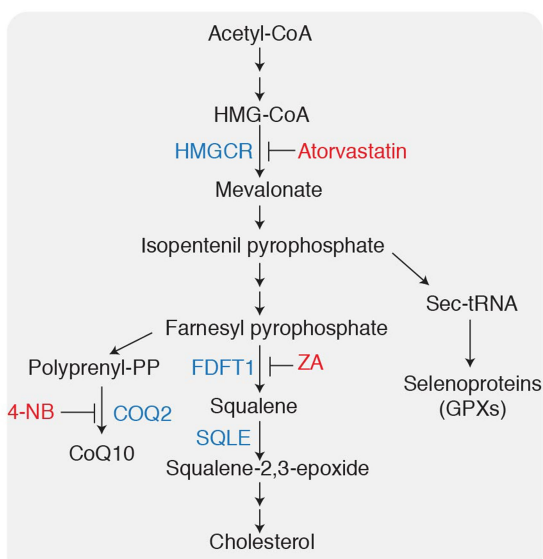
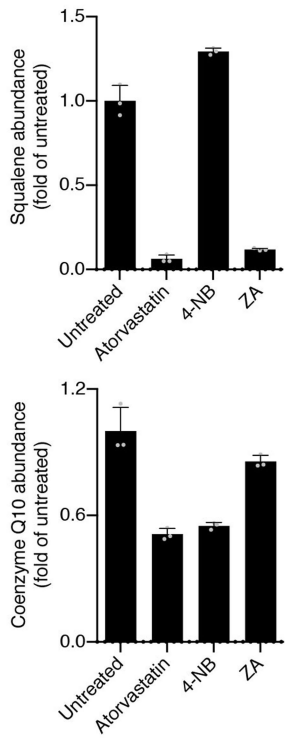
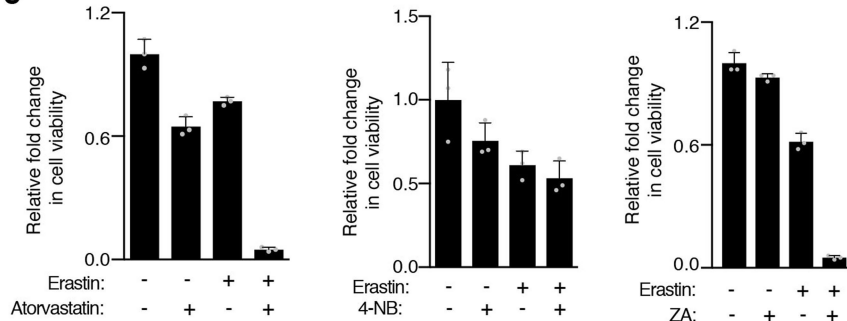
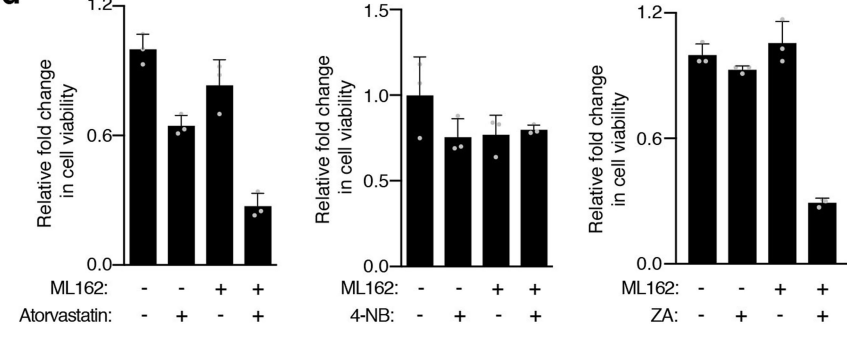
for CCLE collection, 5 independent cell lines for ALCL). **d**, Immunoblot of *LDLR* in the indicated primary PDXs (top). Immunoblotting of *NPC1* in control and ALK⁺ ALCL cell lines (bottom). Actin is included as a loading control. PTCL, peripheral T cell lymphoma. **e**, Immunoblotting of SREBP-2 (non-cleaved and cleaved forms) in cytoplasmic and nuclear fractions of indicated cell lines expressing a vector or an *SQLE* cDNA. The cells were incubated for 24 h in medium containing either FBS (−) or LPDS (+). GAPDH and histone H3 were used as cytoplasmic and nuclear loading controls respectively.



Extended Data Fig. 6 | See next page for caption.

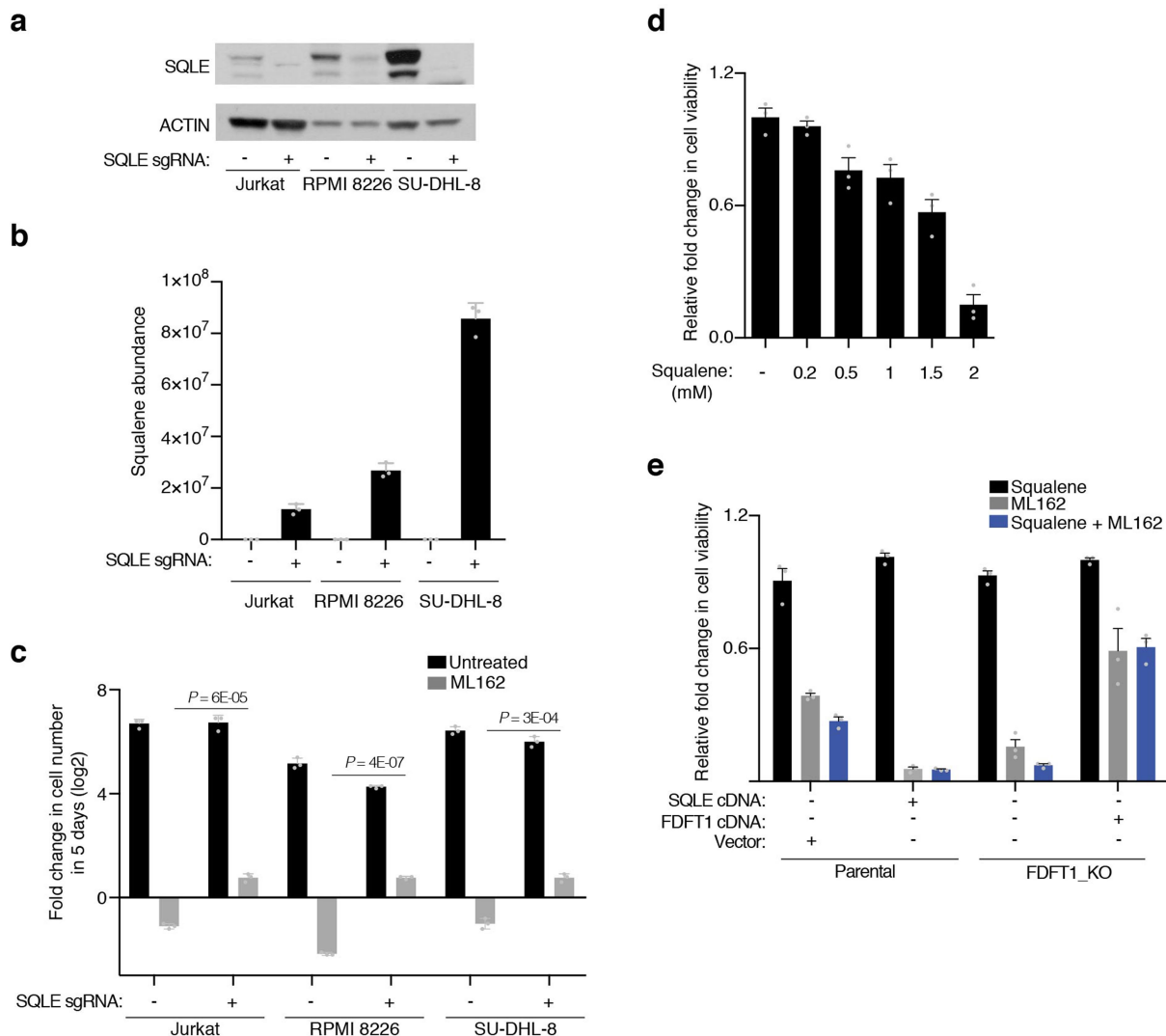
Extended Data Fig. 6 | Squalene accumulation leads to resistance of SQLE-null cells to ferroptosis inducers. **a**, Immunoblots of FDFT1 and SQLE in the indicated Karpas299 cell lines. Actin was used as the loading control. **b**, SRS imaging of squalene for indicated Karpas299 cells. Grey image shows cellular background ($1,372\text{cm}^{-1}$), squalene image (pseudo-coloured yellow hot, $1,386\text{ cm}^{-1}$; left). SRS spectra integrating intensity from lipid droplet with Raman peak of squalene ($1,386\text{ cm}^{-1}$; right) (mean \pm s.d., $n = 3$ biologically independent samples). Error bar represent standard deviation from multiple lipid droplets in at least three cells. **c**, sgRNA competition assay using a pool of five control (sgControl) and five *FDFT1*-targeting (sgFDFT1) sgRNAs in indicated PDXs. Transduced cells were injected subcutaneously to NSG mice to generate tumours. Subsequent to four weeks of growth, genomic DNA was collected to measure sgRNA abundance by deep sequencing. Average guide scores of tumours were calculated and graphed. **d**, Relative fold change in cell viability of indicated Karpas299 lines treated with or without ML162 (20 nM, top) or RSL3 (30 nM, bottom) in the presence or absence of an

SQLE inhibitor (1 μM) for 5 days. **e**, Fold change in cell viability relative to untreated cells of indicated Karpas299 lines treated with or without ML162 (120 nM) for 2 days (top). Representative bright-field micrographs of indicated Karpas299 cells after two days of indicated treatments (bottom). **f**, Immunoblotting of FDFT1 in the indicated DEL and SUP-M2 cell lines. Actin is used as a loading control (left). Relative fold change in cell viability of control, FDFT1-null and rescued DEL and SUP-M2 cell lines in the presence and absence of ML162 (20 nM) after 5 days. **g**, Immunoblotting of FDFT1 in the indicated HEC1B and SNU-1 cell lines. Actin is used as a loading control (top). Squalene abundance of the indicated cell lines (middle). Relative fold change in cell viability of control and FDFT1-null HEC1B and SNU-1 cell lines in the presence and absence of ML162 (200 nM for HEC1B lines, 1 μM for SNU-1 cell lines) and grown for 5 days. In **c–g**, bars represent mean \pm s.d. For **c**, $n = 5$ independent sgRNAs targeting a control region or LDLR gene. For **d–g**, $n = 3$ biologically independent samples. Statistical significance was determined by two-tailed unpaired *t*-test.

a**b****c****d**

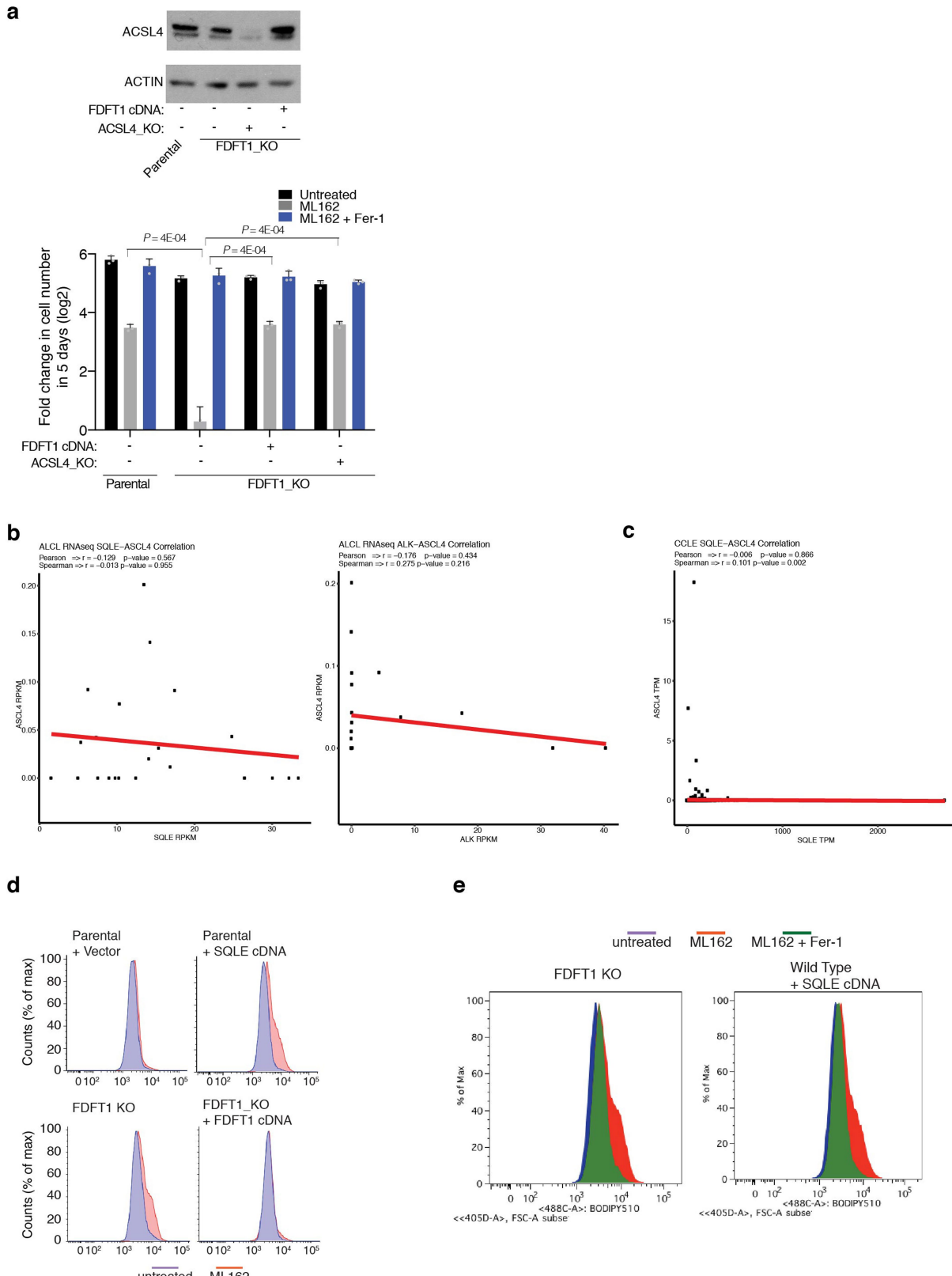
Extended Data Fig. 7 | Blocking squalene accumulation sensitizes ALCLs to a GPX4 inhibitor (ML162) and erastin. **a**, Mevalonate pathway in mammalian cells and fates of the side reactions. Reactions catalysed by HMGCR, COQ2, FDFT1 and SQLE, and chemical inhibitors of these enzymes, are indicated. **b**, Relative abundance of squalene and coenzyme Q10 in Karpas299 treated for 24 h with atorvastatin (1 μ M), 4-nitrobenzoate (4-NB, 1 mM) or zaragozic acid (ZA, 20 μ M) to untreated. **c**, Relative fold change in cell viability of Karpas299 cells treated with

erastin (1 μ M), atorvastatin (1 μ M), 4-nitrobenzoate (4-NB, 1 mM), zaragozic acid (ZA, 20 μ M) or a combination of two of them after 5 days to untreated. **d**, Relative fold change in cell viability compared to untreated cells of Karpas299 cells treated with ML162 (25 nM), atorvastatin (1 μ M), 4-nitrobenzoate (4-NB, 1 mM), zaragozic acid (ZA, 20 μ M) or a combination of 2 of them after 5 days. In **b-d** bars represent mean \pm s.d. For **b-d**, $n = 3$ biologically independent samples.



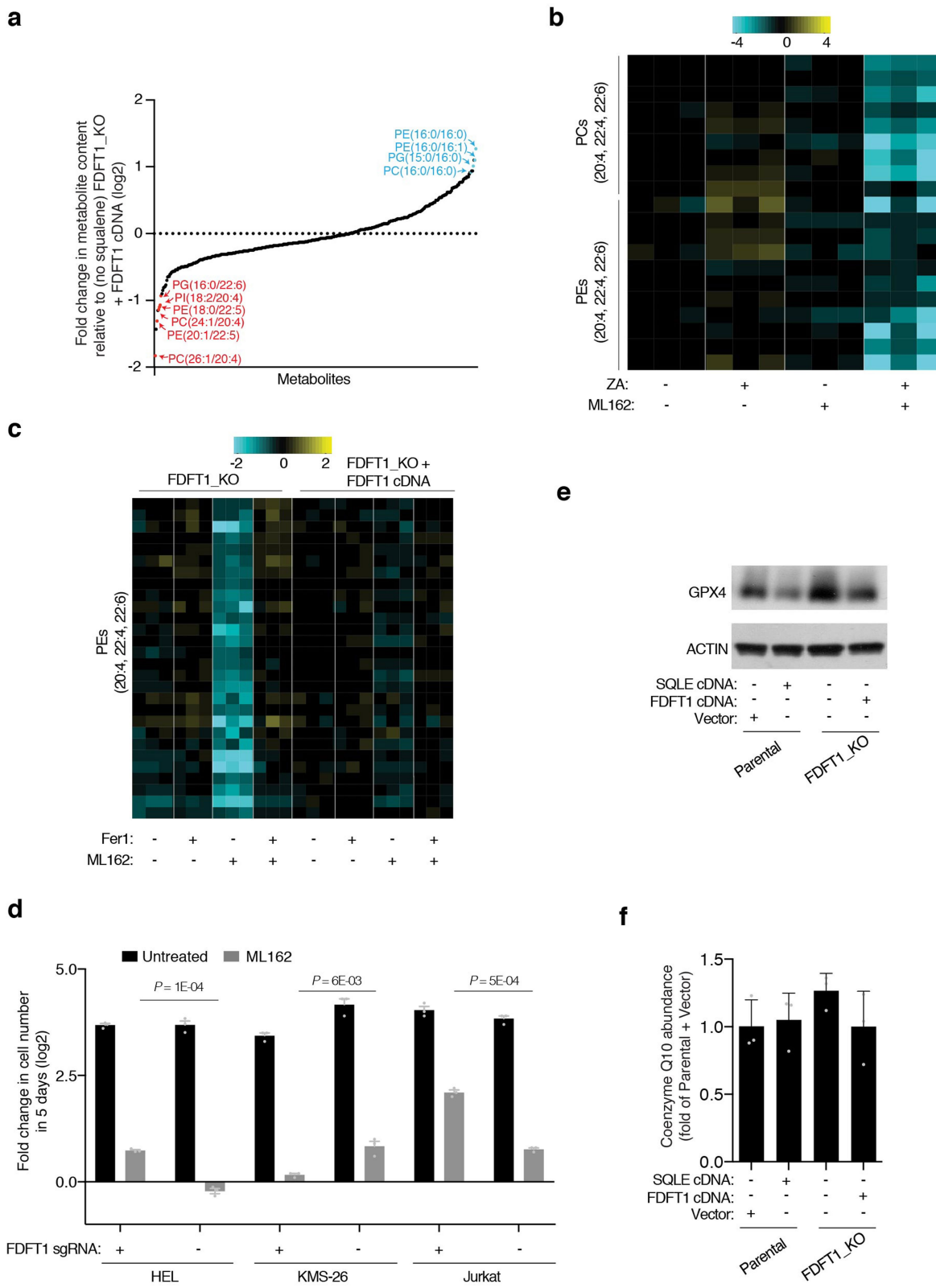
Extended Data Fig. 8 | Loss of SQLE decreases sensitivity of cancer cell lines to ferroptosis inducers. **a**, Immunoblotting of SQLE in the indicated cell lines transduced with a vector or sgSQLE. Actin is used as a loading control. **b**, Squalene abundance in the indicated cell lines. **c**, Relative fold change in cell viability of control and sgSQLE-expressing cell lines in the presence and absence of ML162 (500 nM for Jurkat lines, 200 nM for RPMI 8226 and SU-DHL-8 cell lines) grown for 5 days. **d**, Relative fold

change in cell viability of Karpas299 parental cells supplemented with the indicated concentrations of exogenous squalene to untreated cells. **e**, Relative fold change in cell viability of Karpas299 parental or FDFT1 null cells expressing a vector, *SQLE* cDNA or *FDFT1* cDNA treated with or without ML162, squalene or both, to untreated cells. In **b–e** bars represent mean \pm s.d. For **b–e**, $n = 3$ biologically independent samples. Statistical significance was determined by two-tailed unpaired *t*-test.



Extended Data Fig. 9 | Inhibition of PUFA synthesis prevents ferroptotic cell death in ALCLs. **a**, Immunoblotting of ACSL4 in the indicated Karpas299 cells. Actin is used as a loading control (top). Relative fold change in cell viability of indicated Karpas299 cell lines in the presence or absence of ML162 (20 nM) and Fer-1 (1 μ M) for 5 days (bottom) (mean \pm s.d., $n = 3$ biologically independent samples). Statistics, two-tailed unpaired t -test. **b**, Correlation of mRNA levels of ACCL4 with SQLE (left) and ALK (right) in primary ALCLs dataset ($n = 22$ biologically

independent samples). **c**, Correlation of mRNA levels of ACCL4 with SQLE in CCLE dataset ($n = 935$ independent cell lines). **d**, Lipid peroxidation assessed by flow cytometry measuring C11-BODIPY fluorescence of indicated Karpas299 cell lines after an 18-h treatment with ML162 (200 nM). Representative data from one of three experiments are shown. **e**, Lipid peroxidation assessed by flow cytometry measuring C11-BODIPY fluorescence of indicated Karpas299 cell lines after an 18-h treatment in the presence and absence of ML162 (200 nM) and Fer-1 (1 μ M).



Extended Data Fig. 10 | See next page for caption.

Extended Data Fig. 10 | Squalene accumulation rewires membrane phospholipid composition. **a**, Unbiased lipidomic analysis of Karpas299 FDFT1-null cell line relative to its rescued isogenic counterpart expressing *FDFT1* cDNA. Fold change (\log_2) in metabolite abundance was graphed and membrane phospholipids containing saturated and polyunsaturated fatty acids are indicated. **b**, Heat map showing fold changes (\log_2) in indicated phosphatidylcholines (PCs) and phosphatidylethanolamines (PEs) of Karpas299 cells cultured for 24 h in the absence or presence of ZA (zaragozic acid, 20 μ M) and ML162 (200 nM) relative to untreated cells. Triplicates of each condition are shown. Colour bar indicates \log_2 change in abundance. **c**, Heat map showing fold changes (\log_2) in indicated phosphatidylethanolamines (PEs) of indicated Karpas299 cell lines

cultured for 24 h with Fer-1 (1 μ M) and ML162 (200 nM). Triplicates of each condition are shown. Colour bar indicates \log_2 change in abundance. **d**, Relative fold change in cell viability of HEL, KMS-26 and Jurkat cell lines expressing vector or an sgRNA targeting *FDFT1* in the presence or absence of ML162 (20 nM) for 5 days. **e**, Immunoblotting of GPX4 in indicated Karpas299 cell lines expressing a vector, *SQLE* cDNA, *FDFT1* cDNA or an sgRNA targeting *FDFT1*. Actin is used as a loading control. **f**, Coenzyme Q10 abundance of indicated Karpas299 cell lines relative to parental cells expressing a control vector. In **d** and **f**, bars represent mean \pm s.d. For **d** and **f**, $n = 3$ biologically independent samples. Statistical significance was determined by two-tailed unpaired *t*-test.

Reporting Summary

Nature Research wishes to improve the reproducibility of the work that we publish. This form provides structure for consistency and transparency in reporting. For further information on Nature Research policies, see [Authors & Referees](#) and the [Editorial Policy Checklist](#).

Statistical parameters

When statistical analyses are reported, confirm that the following items are present in the relevant location (e.g. figure legend, table legend, main text, or Methods section).

n/a Confirmed

- The exact sample size (n) for each experimental group/condition, given as a discrete number and unit of measurement
- An indication of whether measurements were taken from distinct samples or whether the same sample was measured repeatedly
- The statistical test(s) used AND whether they are one- or two-sided
Only common tests should be described solely by name; describe more complex techniques in the Methods section.
- A description of all covariates tested
- A description of any assumptions or corrections, such as tests of normality and adjustment for multiple comparisons
- A full description of the statistics including central tendency (e.g. means) or other basic estimates (e.g. regression coefficient) AND variation (e.g. standard deviation) or associated estimates of uncertainty (e.g. confidence intervals)
- For null hypothesis testing, the test statistic (e.g. F , t , r) with confidence intervals, effect sizes, degrees of freedom and P value noted
Give P values as exact values whenever suitable.
- For Bayesian analysis, information on the choice of priors and Markov chain Monte Carlo settings
- For hierarchical and complex designs, identification of the appropriate level for tests and full reporting of outcomes
- Estimates of effect sizes (e.g. Cohen's d , Pearson's r), indicating how they were calculated
- Clearly defined error bars
State explicitly what error bars represent (e.g. SD, SE, CI)

Our web collection on [statistics for biologists](#) may be useful.

Software and code

Policy information about [availability of computer code](#)

Data collection

For mass spectrometry: XCalibur v2.2 (Thermo Scientific) and Skyline.

Data analysis

GraphPad PRISM 7, Microsoft Excel 15.21.1 and FlowJo v.10.

For manuscripts utilizing custom algorithms or software that are central to the research but not yet described in published literature, software must be made available to editors/reviewers upon request. We strongly encourage code deposition in a community repository (e.g. GitHub). See the Nature Research [guidelines for submitting code & software](#) for further information.

Data

Policy information about [availability of data](#)

All manuscripts must include a [data availability statement](#). This statement should provide the following information, where applicable:

- Accession codes, unique identifiers, or web links for publicly available datasets
- A list of figures that have associated raw data
- A description of any restrictions on data availability

Source data for barcoding experiment in Fig. 1 is provided as Supplementary Table 1. Gene scores of CRISPR screens in Fig. 3 and Extended Data Fig. 4 are provided as Supplementary Table 4. Clinical data of Patient Derived Xenografts used in Fig. 3F and Extended Data Fig. 6C is provided as Supplementary Table 5. Source Data

for Figs. 1–4 and Extended Data Figs. 1–10 are available with the online version of the paper. All other data supporting the findings of this study are available from the corresponding author on reasonable request.

Field-specific reporting

Please select the best fit for your research. If you are not sure, read the appropriate sections before making your selection.

Life sciences Behavioural & social sciences Ecological, evolutionary & environmental sciences

For a reference copy of the document with all sections, see nature.com/authors/policies/ReportingSummary-flat.pdf

Life sciences study design

All studies must disclose on these points even when the disclosure is negative.

Sample size	All the experiments were performed using sample sizes based on standard protocols in the field. For primary tumor samples and Patient Derived Tumor Xenografts (PDTXs), sample size depended on the availability of patient samples for each cancer subset as provided by our collaborator.
Data exclusions	No data was excluded in any case.
Replication	All the <i>in vitro</i> experiments were replicated with similar outcome at least 3 times. Both technical and biological replicates were reliably reproduced. <i>In vivo</i> experiments were reproduced at least twice.
Randomization	Sample groups were allocated randomly.
Blinding	The investigator(s) were not blinded during data collection or analysis. For <i>in vivo</i> experiments, blinded researchers performed the injections.

Reporting for specific materials, systems and methods

Materials & experimental systems

n/a	Involved in the study
<input checked="" type="checkbox"/>	<input type="checkbox"/> Unique biological materials
<input type="checkbox"/>	<input checked="" type="checkbox"/> Antibodies
<input type="checkbox"/>	<input checked="" type="checkbox"/> Eukaryotic cell lines
<input checked="" type="checkbox"/>	<input type="checkbox"/> Palaeontology
<input type="checkbox"/>	<input checked="" type="checkbox"/> Animals and other organisms
<input type="checkbox"/>	<input checked="" type="checkbox"/> Human research participants

Methods

n/a	Involved in the study
<input checked="" type="checkbox"/>	<input type="checkbox"/> CHIP-seq
<input type="checkbox"/>	<input checked="" type="checkbox"/> Flow cytometry
<input checked="" type="checkbox"/>	<input type="checkbox"/> MRI-based neuroimaging

Antibodies

Antibodies used

Antibody, catalog number and reference describing the monoclonal LDLR antibody are included in the manuscript.

SQLE (Protein Tech, 12544-1-AP, Lot 00003286, Immunoblotting, 1:1000)

SQLE (Atlas Antibodies, HPA020762, Lot R09745, Immunohistochemistry, 1:200)

Beta-actin (GeneTex, GTX109639, Lot. 42810, 1:10000), ACSL4 (GeneTex, GTX100260, Lot. 39568, 1:1000), GAPDH (GeneTex, GTX627408, Lot. 41323, 1:1000), LDLR (Abcam, ab52818, Lot. GR295148-7, 1:500), NPC1 (Abcam, ab36983, 1:1000)

GPX4 (Abcam, ab41787, Lot. GR56784-1, 1:250), FDFT1 (Protein Tech, 13128-1-AP, Lot. 00044214, 1:1000), ALK (CST, C26G7, 1:1000), STAT3 (CST, 9132), Phospho-STAT3 (CST, 9131), Histone H3 (CST, 4499S, Lot. 9, 1:500).

Secondary Antibodies:

HPR-conjugated Mouse Anti-Rabbit IgG (Santa Cruz, sc-2357, Lot. No. L0617, 1:5000).

HPR-conjugated Donkey Anti-Mouse IgG (Santa Cruz, sc-2096, Lot. No. J2315; 1:5000).

Validation

Each antibody used in this work was validated prior to its use following manufacturer's instructions.

Eukaryotic cell lines

Policy information about [cell lines](#)

Cell line source(s)	All cell lines used in this study were purchased from ATCC and DSMZ or a gift of Sabatini and Weinberg labs.
Authentication	Short Tandem Repeat (STR) profiling of all the cell lines used in this work was performed in collaboration with the Integrated Genomics Operations Center in Memorial Sloan Kettering Cancer Center.
Mycoplasma contamination	PCR analysis confirming the absence of mycoplasma contamination was performed routinely every 6 months.
Commonly misidentified lines (See ICLAC register)	Two of the cell lines used in this study are reported in ICLAC as misidentified cell lines but included in our analysis for diversity due to their oncogene status and metabolic phenotypes: U-937 is a rare histiocytic lymphoma cell line described as auxotrophic for cholesterol, and NCI-H929 is a myeloma cell line with low GLUT3 expression.

Animals and other organisms

Policy information about [studies involving animals; ARRIVE guidelines](#) recommended for reporting animal research

Laboratory animals	All animal studies and procedures were conducted according to a protocol approved by the Institutional Animal Care and Use Committee (IACUC) at the Rockefeller University and another one at Well Cornell Medicine for the Patient Derived Tumor Xenograft model. Male and female 6-14 weeks old NOD scid gamma (NSG) mice (Taconic) were used.
Wild animals	This study did not involve the use of wild animals.
Field-collected samples	This study did not involved the use of field-collected samples.

Human research participants

Policy information about [studies involving human research participants](#)

Population characteristics	We provided a supplementary table (Supplementary Table 5) regarding patient information. Briefly, samples IL69 and IL79 (ALK+ PDX1 and ALK+ PDX3 in Fig. 3h) correspond to patients who experience a refractory clinical course unresponsive to standard chemo-immunotherapy. IL69 correspond to a 20-year-old male diagnosed with ALK+ ALCL of the right shoulder, who received 2 cycle of CHOP followed by two additional 3 cycles of BV-CHP. On progressive disease, the patient was treated with Crizotinib but he died with active systemic disease and CNS involvement after a month. IL79 was a 65-year-old male with a relapsed ALK+ ALCL treated with BV-CHOP vs CHOP, who also died with progressive disease after 4 month of therapy (Supplementary Table 5). Fresh and/or viable cryopreserved samples from primary ALCL were obtained at the time of diagnosis, before treatment, or at relapse after chemotherapy. Formalin Fixed Paraffin Embedded tissue samples were obtained from multiple institutions and the diagnoses were rendered according to the WHO classification. Review of samples were performed in blind by two experienced pathologists to determine the percentage of lymphoma cells, based on H&E and immunohistochemistry (CD30 etc.). Only samples with more than 50% of tumor cells were selected for further analyses. Representative formalin-fixed tumor sections and/or tissue microarrays (TMAs) were processed for immunohistochemical (IHC) analyses on a semi- automated stained. Informed consents were obtained following the recommendations of local ethical committees.
Recruitment	See above.

Flow Cytometry

Plots

Confirm that:

- The axis labels state the marker and fluorochrome used (e.g. CD4-FITC).
- The axis scales are clearly visible. Include numbers along axes only for bottom left plot of group (a 'group' is an analysis of identical markers).
- All plots are contour plots with outliers or pseudocolor plots.
- A numerical value for number of cells or percentage (with statistics) is provided.

Methodology

Sample preparation	Indicated cancer cell lines were plated (250,000 cells/well) in 6-well plates and treated with ML162 for 18 hrs prior to two washes with HBSS and incubation of cells in 500 uL of HBSS containing BODIPY 581/591 C11 (1 uM). After 15 min incubation at 37 °C, cells were washed twice on ice-cold HBSS and resuspended in 0.5 mL of HBSS containing 50ng/ml DAPI and filtered into FACS tubes with cell-strainer cap.
Instrument	BD LSR II Flow Cytometer (BD Biosciences)
Software	FlowJo v.10

Cell population abundance

N/A

Gating strategy

Live cells were selected from the starting cell population on a DAPI/FSC-A plot.
Then, single cells were selected using a FSC-A/FSC-H plot from the population of live cells. Data displayed represents populations of live, singlet cells.

Tick this box to confirm that a figure exemplifying the gating strategy is provided in the Supplementary Information.